



## Original Paper

# Dynamic evolution characteristics of the “source-reservoir” integration of gray marl and its geological significance to unconventional gas: Insights from pyrolysis experiments



Zhang-Hu Wang<sup>a, b</sup>, Zhong-Liang Ma<sup>c, d, \*</sup>, Lun-Ju Zheng<sup>c, d</sup>, Jun-Yu Wang<sup>c, d</sup>, Zhi-Gang Wen<sup>a, b</sup>, Chen-Yang Si<sup>e</sup>

<sup>a</sup> Cooperative Innovation Center of Unconventional Oil and Gas, Yangtze University, Wuhan, Hubei, 430100, China

<sup>b</sup> Key Laboratory of Oil and Gas Resources and Exploration Technology, Ministry of Education, College of Resources and Environment, Yangtze University, Wuhan, Hubei, 430100, China

<sup>c</sup> Wuxi Research Institute of Petroleum Geology, Sinopec Exploration and Production Research Institute, Wuxi, Jiangsu, 214126, China

<sup>d</sup> State Key Laboratory of Shale Oil and Gas Enrichment Mechanisms and Effective Development, Wuxi, Jiangsu, 214126, China

<sup>e</sup> School of Metallurgy and Environment, Central South University, Changsha, Hunan, 410083, China

## ARTICLE INFO

## Article history:

Received 4 August 2022

Received in revised form

25 September 2022

Accepted 6 January 2023

Available online 7 January 2023

Edited by Jie Hao and Teng Zhu.

## Keywords:

Residual oil

Organic pores

Porosity

Sepiolite

Hydrocarbon generation

## ABSTRACT

The marl–limestone rhythmic strata of the Permian Maokou Formation have been identified as hosts of unconventional gas reservoirs with “source–reservoir” integration. The lack of research on the pore structure evolution of organic-rich carbonate rock restricts gas exploration of these strata. Here, pyrolysis experiments were performed on the Mao-1 carbonate to simulate hydrocarbon generation, expulsion and diagenesis in gray marl from low maturity to overmaturity. The pore structure of this marl is dominated by mesopores and macropores, and the proportion of macropores increases gradually with temperature. The macropores are mainly pores in the organic matter and shrinkage microcracks. Additionally, micropores and mesopores, dominated by clay mineral interlayer pores and pyrite intergranular pores, are developed in the high mature stage and subsequently compressed in the overmature stage. The main contributors to the specific surface area are micropores and mesopores, which are conducive to natural gas adsorption. After the same pyrolysis treatment, the available porosity of grey marl is higher than that of marine/lacustrine shales, and exhibits an obvious decrease in the low mature–mature stage. These suggest that the abundant residual oil generated blocked the organic and inorganic pores in the gray marl, providing a pivotal material foundation for the gas generation. Micropores and mesopores developed during the high mature stage ensure the gas accumulation and preservation. The above indicate the organic-rich carbonate at the high mature–overmature stage ( $R_o = 1.7\%–2.5\%$ ) in the Sichuan Basin may be a favorable exploration horizon for unconventional oil and gas.

© 2023 The Authors. Publishing services by Elsevier B.V. on behalf of KeAi Communications Co. Ltd. This is an open access article under the CC BY-NC-ND license (<http://creativecommons.org/licenses/by-nc-nd/4.0/>).

## 1. Introduction

Unconventional gas reservoirs are characterized by the presence of adsorbed or free gas in organic-rich shale and carbonate with limited porosity and permeability (Curtis, 2002; Jarvie et al., 2007; Garcia et al., 2018; Kuang et al., 2022). At present, research on unconventional oil and gas reservoirs in China is mainly focused on

marine shale gas (Song et al., 2015; Chen et al., 2017; Sun et al., 2017; Liu et al., 2019; Wang et al., 2020; Zhao et al., 2020). However, few studies have focused on unconventional carbonate gas, although the predicted unconventional carbonate petroleum and gas resources in China are  $3.4 \times 10^{10}$  t and  $2.4 \times 10^{13}$  m<sup>3</sup>, respectively (Ma et al., 2017), suggesting that organic-rich carbonates have abundant oil and gas potential. In recent years, several oil and gas fields have been discovered in carbonate, i.e., the Cambrian–Ordovician carbonate in the Tarim Basin, the Ordovician carbonate in the Ordos Basin, and the Triassic and Permian carbonates in the Sichuan Basin. The Mao-1 Member, which consists of gray marl–limestone rhythmic strata, of the Permian Maokou

\* Corresponding author. Wuxi Research Institute of Petroleum Geology, Sinopec Exploration and Production Research Institute, Wuxi, 214126, China.

E-mail address: [mazl.syky@sinopec.com](mailto:mazl.syky@sinopec.com) (Z.-L. Ma).

Formation (Fig. 1) is widely developed in Sichuan, Guizhou, and Hunan provinces (Li et al., 2021a). The Mao-1 gray marl is an important source rock and is conducive to oil and gas accumulation (Zhou et al., 2016; Liu et al., 2021). Recently, several wells (YY1, JH1, TT1, B23, and WJ1) reached industrial gas flow levels in this set of strata. Among them, the B23 well has the highest production rate of  $5.1 \times 10^5 \text{ m}^3/\text{d}$  (Fig. 1a, Su et al., 2021). The Mao-1 carbonate has been identified as a new formation containing unconventional gas reservoirs with “source–reservoir” integration (Li et al., 2021b). However, there are few studies on hydrocarbon generation, expulsion, and pore evolution in organic-rich marls, which restricts oil and gas exploration in this rock type.

In general, hydrocarbon generation, expulsion, and diagenesis (i.e., compaction, cementation, transformation, and dissolution of clay minerals) are the primary factors influencing the formation of pore systems in organic-rich carbonate rocks (Verwer et al., 2011; Lei et al., 2015; Tang et al., 2021). Similar to shale reservoirs, the pore system of carbonates is composed of organic pores and inorganic (mineral) pores (Lucia, 1983; Lønøy, 2006). The inorganic porosity is attributed to the mineral composition of the marl, which is generally composed of mainly calcite, dolomite and clay minerals. Therefore, changes in mineral content may affect the rock mechanical properties, pore structure, and gas storage capacity (Ross and Bustin, 2007; Pommer and Milliken, 2015). The total organic carbon (TOC) content and kerogen type affect the pore volume and specific surface area of organic pores, while the thermal evolution of organic matter controls the formation of various pores (Liu et al., 2017; Li et al., 2019a; Wang and Guo, 2021). In the actual geological burial process, there is currently no consensus on the quantitative details of the formation and evolutionary characteristics of carbonate pore systems and their effect on the accumulation of hydrocarbons. This is a popular but challenging topic in the relevant research.

Shale reservoirs are characterized by the following: (1) In the process of kerogen hydrocarbon generation, the pore types of shale

are mainly mesopores and micropores, and the pore volume range is relatively narrow. (2) The formation of fractures is mainly related to the lithostatic pressure, brittleness intensity, and bedding type, thus affecting the storage preservation capacity of shale gas. Under preservation conditions, due to the development of laminae bedding, shale is easily deformed and distorted under tectonic stress, and shale hydrocarbon gas reservoirs can be destroyed. (3) In oil exploitation, shale reservoirs generally have low porosity and low permeability, with higher paraffins and poor fluidity of crude oil, making these reservoirs difficult to exploit (Chen et al., 2018a; Bai et al., 2022). However, compared with shale reservoirs, carbonate reservoirs (1) are more susceptible to the influence of organic acids and can develop mesopores and macropores, which are more conducive to the accumulation of hydrocarbons (Schieber, 2010; Radwan et al., 2021); (2) have a high content of rigid minerals and strong particle support, resulting in a stronger anti-destructive ability (Ma et al., 2018); and (3) can further expand the rock pore space through vertical well acidification, which is more conducive to exploitation (Li et al., 2018).

Comparisons of the pore characteristics of natural shale samples (Mastalerz et al., 2013; Klaver et al., 2015; Topór et al., 2017) to shale samples subjected to various temperatures via pyrolysis experiments (Ko et al., 2016; Guo et al., 2017; Wang and Guo, 2019; Liu et al., 2022) have been successfully used to analyze the pore evolution of the whole pyrolysis series from low maturity to over-maturity. Organic-rich carbonates are widely distributed and deeply buried in the Sichuan Basin, South China. The kerogen in this rock is basically high mature or overmature and has good petroleum generation potential (Zhou et al., 2016; Li et al., 2021a). Here, an organic-rich marl with low maturity from the Mao-1 Member in Guangyuan city, Sichuan Province (Fig. 1), was selected for semi-closed pyrolysis experiments. The goals of this study are to observe and compare the microcharacteristics of naturally and artificially matured samples to provide insight into the dynamic evolution characteristics of source–reservoir integration and provide

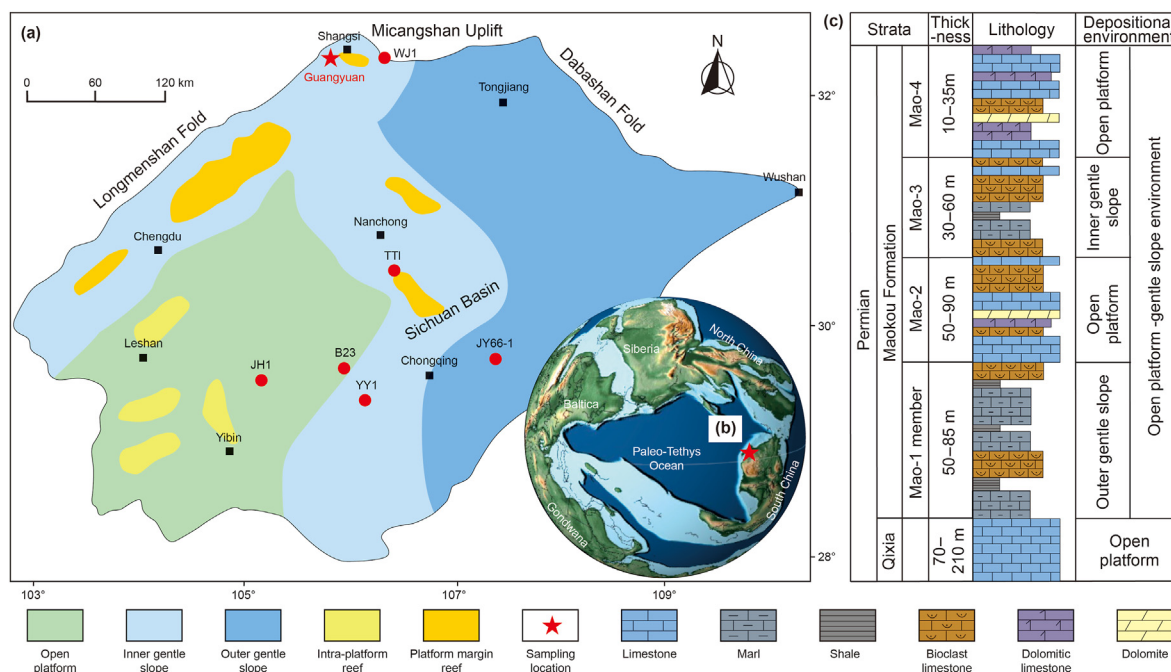


Fig. 1. Geological settings. (a) Paleogeographic maps of the Sichuan Basin during the early Permian. (b) Global paleogeographic reconstruction of the early Permian (260 Ma). (c) Lithology of the Maokou Formation corresponding to the depositional environment in Guangyuan city, Sichuan Province.

evaluation parameters for further unconventional carbonate exploration.

## 2. Geological setting

In the early Permian, South China was located near the equator, adjacent to the Paleo-Tethys Ocean to the west and the Panthalassa Ocean to the east (Fig. 1b). The Sichuan Basin is a primary tectonic unit on the northwestern margin of South China (Jia et al., 2006; Li et al., 2019b). From the bottom up, the Permian strata are the Liangshan, Qixia, and Maokou formations (Fig. 1c). During the sedimentary period of the Liangshan Formation, the environment produced shore/swamp facies, and the lithology was dominated by gray–black shales with multiple sets of coal seams. Subsequently, the depositional environment transitioned into an open platform facies due to a transgressive event during the sedimentary period of the Qixia Formation (Wei et al., 2010). The Sichuan Basin experienced rapid transgression and then slow retrogression during the sedimentary period of the Maokou Formation, resulting in carbonate platform/gentle slope facies. Generally, the Maokou Formation is also regarded as a complete depositional cycle and can be divided into four members (i.e., the Mao-1, Mao-2, Mao-3, and Mao-4 members, Fig. 1c). The Mao-1 Member constitutes a transgressive system tract, while the Mao-2 to –4 members are composed of regressive system tracts (Su et al., 2015; Yang et al., 2015). The depositional environment of the Mao-1 Member was dominated by gentle slope conditions, and the lithology was mainly gray marl and bioclastic limestone, which formed rhythmic bedding and exhibited an “eyeball structure”. The Mao-1 gray marl is regarded as an important source rock in the Sichuan Basin. Due to the change in sea level, the depositional conditions of the Mao 2–4 members gradually transformed to carbonate platform conditions, and were dominated by bioclastic limestone and dolomitic limestone (Tang et al., 2016).

The organic-rich marl of the Mao-1 Member in the Sichuan Basin has mainly entered a high mature–overmature stage, mainly producing natural gas, but in some areas, the source rocks are of low maturity (Su et al., 2021). The thermal evolution of the Mao-1 gray marl varies greatly and is usually lower in the uplift zone and higher in the depression zone (Hu et al., 2021). Previous studies have suggested that the hydrocarbon-generating materials of the source rocks in the Mao-1 Member are phytoplankton and benthic algae (Li et al., 2012; Zhang et al., 2021).

## 3. Materials and methods

The Mao-1 sample selected was mainly from the Shangsi section, Guangyuan city, Sichuan Province. The section was close to the Longmenshan Fold, with a shallow burial depth and low maturity of source rocks. The sampling location was at the bottom of the Maokou Formation (Fig. 1c). We drilled 9 cylindrical samples from the same layer in the Mao-1 marl. Each sample was cut into cylindrical samples (3.5 cm diameter) and less than 2 cm apart to ensure that the mineral composition and TOC content were not heterogeneous. In addition to one natural sample retained as a reference, the other 8 samples were subjected to pyrolysis experiments to simulate the pore characteristics at different maturity stages.

### 3.1. Pyrolysis experiment

The experiment was conducted in a high-temperature and high-pressure semiclosed hydrous pyrolysis hydrocarbon generation and expulsion pyrolysis system at the Wuxi Research Institute of Petroleum Geology (Fig. 2). The high-temperature pyrolysis experiment on the gray marl of the Mao-1 Member was carried out under

static rock pressure and formation fluid pressure conditions similar to geological conditions. The whole instrument is composed of four devices, i.e., a reaction device under high temperature and pressure conditions, a hydrocarbon expulsion separation and collection device, an oil–gas separation and collection device, and a data collection and automatic device (Fig. 2). For additional information on each device, please see (Ma et al., 2021).

First, according to the burial evolution of the Maokou Formation at well JY66-1 as a geological constraint, the burial depth, static rock pressure, and formation fluid pressure corresponding to the vitrinite reflectance ( $R_o$ ) were confirmed (Table 1). Then, the temperature was set at 8 temperature points, ranging from 300 to 550 °C, including the hydrocarbon evolution stages from low maturity to overmaturity. One sample was tested at each temperature point. Before the operation of the instrument, the reaction device was checked for leaks and then vacuumed, water was added, and the reaction system was heated according to the set parameters; the oil, gas and residual products were collected after the reaction was completed. During the experiment, hydrocarbons were expelled into the product separation and collection subsystem. Some of the samples were split for use in the determination of TOC content and  $R_o$ . The residue from the remaining samples was extracted for 72 h by using organic solvent to measure the residual oil in the gray marl after heating. The gases were collected in the oil–gas separation and collection device.

### 3.2. Organic geochemistry

To measure the TOC content, 100 mg samples were first treated with excess hydrochloric acid solution (volume ratio 1:7) and then washed with distilled water to remove the chlorides. The TOC content was determined by using a high-frequency infrared carbon and sulfur analyzer (LECO CS-744). An electronic microscope setup comprising a Zeiss Axio imager and an MSP200 photometer was used to determine  $R_o$ . The magnification was set to 500 xs. Under white light, the solid residue was examined with an oil immersion objective lens and a 546 nm filter. The index of refraction was 1.518 at 23 °C. Each sample's  $R_o$  was based on an average of 30 measurements.

### 3.3. Low-pressure $N_2$ gas adsorption and porosity measurement

After the experiments, the samples were crushed to below 80 mesh, and each sample was degassed in a vacuum chamber at 110 °C for 6 h to remove the adsorbed water and volatile substances. Then, under the condition of a low temperature of 77.3 K and relative pressure  $p/p_o$  of 0.05–0.35 ( $p$  is the equilibrium pressure, and  $p_o$  is the saturation pressure), the Brunauer–Emmett–Teller (BET) calculation model was used to analyze the multipoint specific surface area. The Barrett–Joyner–Halenda (BJH) model was used to compute pore size and pore volume, and the pore size ranged from 1 to 120 nm with a  $p/p_o$  of 0.06–0.99. The calculation results of the above two models were automatically generated by computer software.

For active porosity measurement, the samples after the experiment were cut into a plunger with a diameter of 2.5 cm and then put into the oven, and the quality was recorded. First, the volume of the sample chamber and the reference chamber of the QK-98 gas porosity tester needed to be calibrated. Then, the samples were placed into the sample chamber, helium gas was injected with a pressure of approximately 1.378 MPa (200 psi), and the pressures in the reference chamber and the sample chamber were recorded. Finally, the connecting valve was opened, and the pressure was allowed to balance before it was recorded. The skeleton volume of the rock was measured with helium gas, and the porosity of the

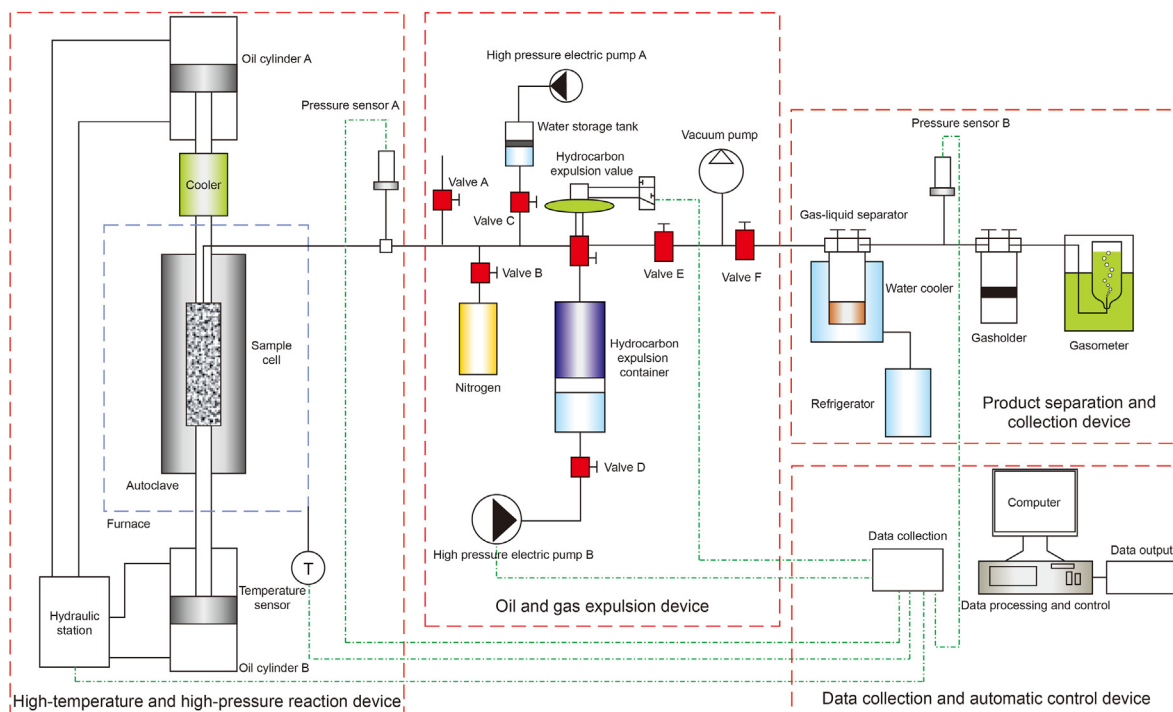


Fig. 2. Semiclosed hydroous pyrolysis experimental device.

Table 1  
Experimental conditions for the pyrolysis experiments of Mao-1 gray marl.

Sample	Simulated temperature, °C	Simulated burial depth, m	Lithostatic pressure, MPa	Minimum formation pressure, MPa	Maximum formation pressure, MPa	Heating rate, °C/min	Keeping time, h
S-1	300	2600	61.15	26.0	39.0	1	48
S-2	330	2900	68.21	29.0	43.5	1	48
S-3	350	3500	82.32	35.0	52.5	1	48
S-4	400	4000	94.08	40.0	60.0	1	48
S-5	425	4050	95.26	40.5	60.8	1	48
S-6	450	4100	96.43	41.0	61.5	1	48
S-7	500	4300	101.14	43.0	64.5	1	48
S-8	550	5500	129.36	55.0	82.5	1	48

rock was then calculated from the total volume and the skeleton volume. The accuracy of the pressure sensor is not less than ±0.0689 kPa (0.01 psi).

### 3.4. Scanning electron microscopy observation

The samples were cut along the vertical bedding plane. After the surface roughness was reduced with an Ar-ion polishing device, the surface was polished with a Leica EM TIC 3X ion beam system. Subsequently, the polished area was sprayed with Au. Field emission scanning electron microscopy (FE-SEM, SIGMA300) was used to examine the samples. Notably, Ar can cause pyrite to be removed from the sample, even near organic matter. When analyzing the pore structures through FE-SEM observations, this phenomenon should be considered (Valentine et al., 2021).

## 4. Results

### 4.1. Hydrocarbon generation and expulsion process

The TOC content of the natural sample is 1.89 w.t.%, the hydrogen index (HI) value is 233 mg HC/g TOC, and the vitrinite reflectance ( $R_o$ ) is 0.54%. The  $R_o$  of the sample after undergoing the

experiment at the highest temperature point (550 °C) reaches 3.1% (Table 2). The whole experimental process included three thermal evolution stages, namely, the low mature–mature stage, the mature–high mature stage, and the high mature–overmature stage, considering the hydrocarbon generation and expulsion process of each stage (Fig. 3).

During the low mature–mature stage, the  $R_o$  of the samples is 0.64–1.13% at temperatures of 300–350 °C. The samples entered the oil generation window at the first temperature point of 300 °C ( $R_o = 0.64%$ ). Although hydrocarbons were first generated in this stage, the expelled oil and gas yields are relatively low at 16.86 kg/tc and 4.74 kg/tc, respectively. In addition, the residual oil yield is relatively high, reaching 154.79 kg/tc. When the temperature is 330–350 °C, the  $R_o$  of the samples is between 0.90% and 1.13%. The total oil yield reaches the highest value (305.33 kg/tc), and the generated oil is mainly residual oil (269.77 kg/tc).

During the mature–high mature stage, the  $R_o$  of the samples is 1.13–1.72% at temperatures of 350–425 °C. The expelled oil yield increases rapidly and peak (126.08 kg/tc). However, the residual oil and total oil yields decrease rapidly and are 43.41 kg/tc and 169.49 kg/tc, respectively, and the yield of hydrocarbon gas continues to rise, reaching 199.06 kg/tc. This stage can be divided into two periods: 350–400 °C and 400–425 °C. When the temperature

**Table 2**  
TOC,  $R_o$ , and pore structure parameters of the samples at different temperatures.

Temperature, °C	TOC, %	$R_o$ , %	Pore volume, cm <sup>3</sup> /kg				BET specific surface area, m <sup>2</sup> /g	Porosity, %
			Micropore	Mesopore	Macropore	Total pore		
Unheated	1.89	0.54	2.50	6.26	4.90	13.66	5.85	7.43
300	1.97	0.64	1.74	9.79	6.59	18.12	4.64	8.28
330	1.75	0.9	1.39	9.01	6.22	16.62	3.48	7.06
350	1.6	1.13	1.59	10.07	5.84	17.50	3.96	5.64
400	1.27	1.54	5.62	26.37	5.36	37.35	14.59	7.74
425	1.22	1.72	5.06	25.27	6.94	37.27	12.86	11.50
450	1.23	2.17	4.71	25.80	9.14	39.65	12.02	13.49
500	1.25	2.79	2.56	13.20	12.40	28.16	6.09	13.19
550	1.16	3.10	2.84	10.86	13.62	27.32	6.84	14.43

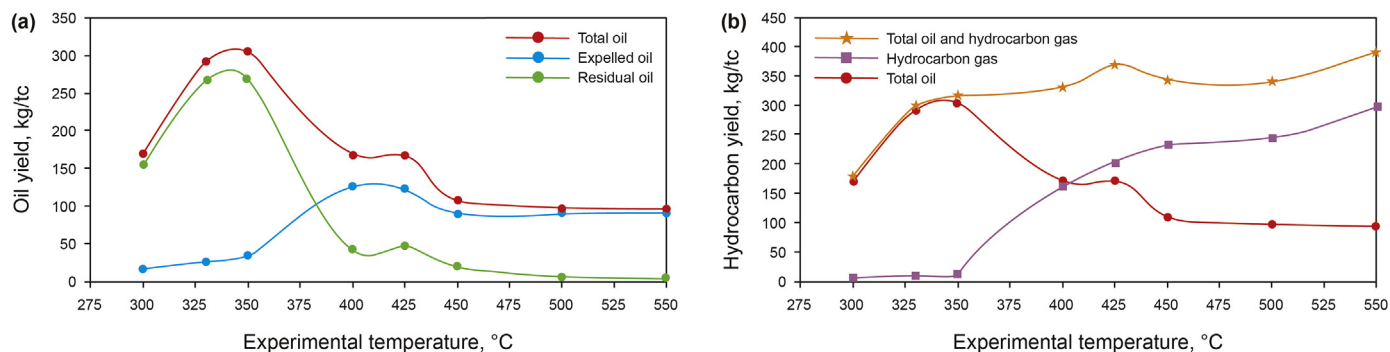


**Fig. 3.** Variation in the characteristics of (a) oil and (b) gas yield at different temperatures.

is 350–400 °C, the TOC content of the gray marl decreases from 1.6 to 1.39%, and kerogen is mainly cracked into crude oil. In addition, the expelled oil yield gradually exceeds the residual oil yield, which suggests that the residual oil generated in the Mao-1 gray marl should have reached the maximum content during this period. When the temperature is 400–425 °C, the yield of hydrocarbon gas gradually exceeds the total oil yield. In addition, although the expelled oil yield also reaches the highest value (126.08 kg/tc), the residual oil content in the sample begins to decline rapidly.

During the high mature–overmature stage, the  $R_o$  of the samples is 1.72–2.17% at 425–450 °C (Table 2). The expelled oil yield starts to gradually decrease (89.35 kg/tc), while the hydrocarbon gas yield continues to rise (233.02 kg/tc). When the temperature is 450–550 °C, the  $R_o$  of the samples ranges from 2.17% to 3.10%. The expelled oil yield and the total oil yield remain basically stable. However, the residual oil yield decreases to the lowest value (0.48 kg/tc), and there is seldom crude oil in the marl. Concurrently, the hydrocarbon gas yield reaches its peak, up to 297.40 kg/tc. In terms of quality, hydrocarbon gas components account for more than 76% of the total hydrocarbons. In this stage, kerogen basically stops cracking, and long-chain liquid hydrocarbons no longer form. The remaining alkyl chains, especially the previously formed light liquid hydrocarbons, continue to crack at high temperatures to generate a large amount of methane.

The highest oil yield is 305 mg/g TOC, and the highest yield of both oil and gas is close to 400 mg/g TOC. Oil and gas production is much greater than the HI value of the natural sample. This is mainly because Rock-Eval is a fully open system that easily produces small-molecule hydrocarbons at 600 °C. However, in a semiclosed hydrocarbon system, water is conducive to the generation of oil (Lewan and Roy, 2011), but a part of the oil discharge system does not continue to crack. The actual hydrocarbon yield is 40%–50% higher than the HI determined from Rock-Eval (Ma et al., 2021).

In the hydrocarbon generation and expulsion process, the TOC content of the gray marl decreases significantly from 1.89% to 1.25%

in the oil generation stage (300–400 °C) and from 1.25% to 1.16% in the gas generation stage (400–550 °C). The oil generation stage was likely the main period of kerogen consumption.

#### 4.2. Porosity and pore structure

The experimental results are given in Table 2. The accessible porosity of the samples ranged from 5.64% to 14.43%, showing an overall increasing trend with temperature. When the sample is at the low mature–mature stage, the porosity at the oil generation window is the largest (8.28%) after 300 °C but decreases from 330 °C to 350 °C. Subsequent temperature increases nearly all result in an increase in porosity to 13.49% rapidly at the mature–high mature stage and reach the maximum value at the overmaturity stage (14.43%).

Observing the low-pressure N<sub>2</sub> gas adsorption–desorption reveals that the adsorption isotherms of the samples at different temperatures belong to type IV (Brunauer et al., 1940; Gregg et al., 1967) and that the pores were developed from micropores ( $d < 2$  nm) and mesopores ( $2 \text{ nm} < d < 50$  nm) to macropores ( $d > 50$  nm). The pore type is dominated by mesopores, followed by macropores and micropores (Table 2). When the relative pressure is greater than 0.45 ( $p/p_o > 0.45$ ), the adsorption and desorption curves of the samples show obvious hysteresis, indicating that capillary condensation has occurred on the surface of the matrix. There are obvious differences in the morphological development and connectivity of pores with different diameters, and the pore structure system is highly heterogeneous (Fig. 4). In addition, according to the IUPAC classification, the hysteresis type of each sample is close to Type H3 (Sing, 1985), indicating a wedge-shaped or parallel-shaped slit-type pore. From low maturity to overmaturity, the adsorption capacity of gray marls increases throughout the 450 °C ( $R_o = 2.17\%$ ) experiment, where it reaches a maximum value before decreasing at higher temperatures.

The pore volume and specific surface area data are shown in

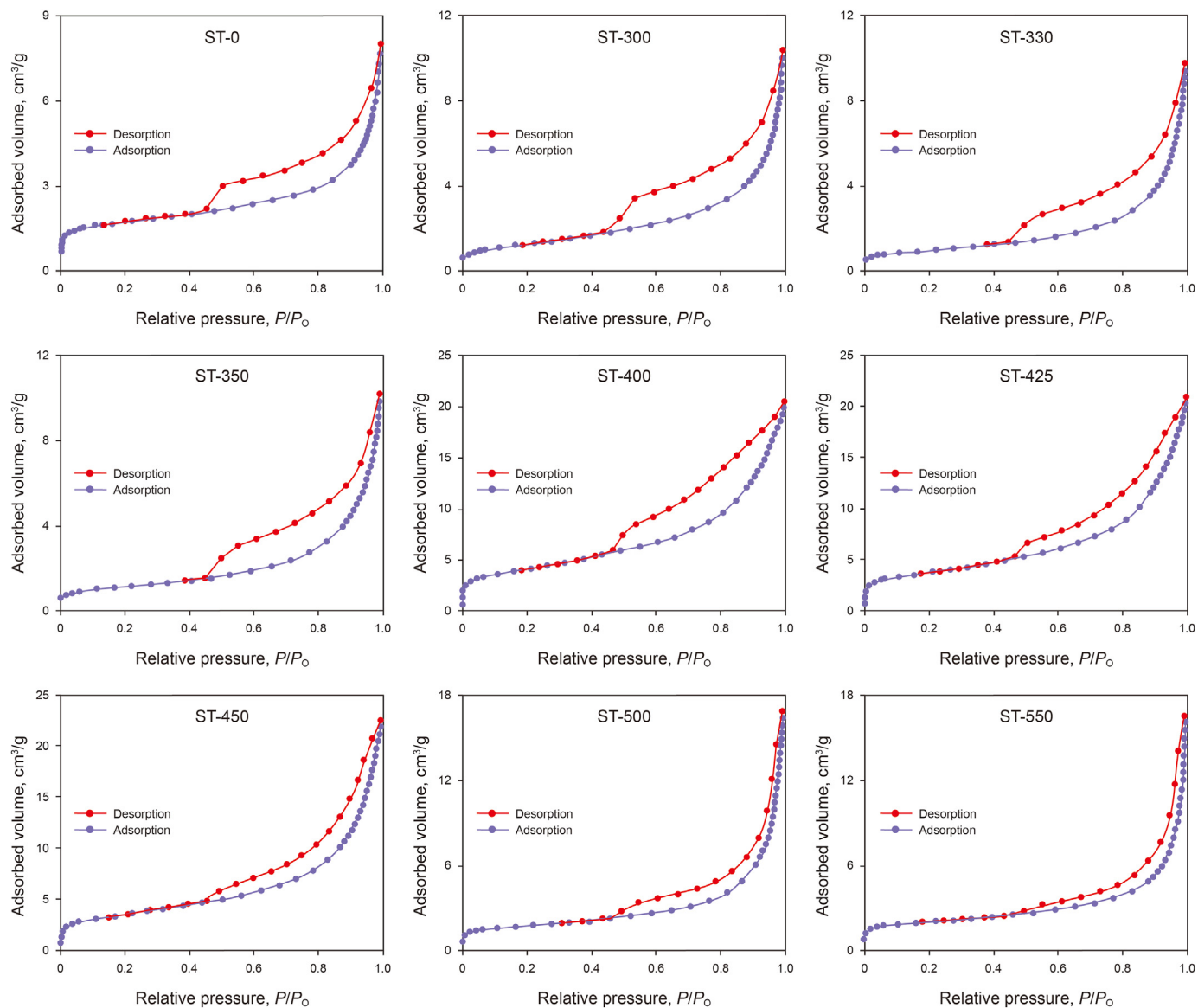


Fig. 4.  $N_2$  adsorption–desorption curves of the simulated gray marl at different temperatures.

**Table 2.** During the low mature–mature stage, the micropore volume and macropore volume remain relatively unchanged, but the mesopore volume ranges from  $6.26 \text{ cm}^3/\text{kg}$  to  $10.07 \text{ cm}^3/\text{kg}$ . During the mature–high mature stage, the micropore volume and mesopore volume increase rapidly from  $1.59$  to  $5.62 \text{ cm}^3/\text{kg}$  and  $10.07$  to  $26.37 \text{ cm}^3/\text{kg}$ , respectively, from  $350 \text{ }^\circ\text{C}$  to  $400 \text{ }^\circ\text{C}$ , while the macropore volume basically remains unchanged. During the high mature–overmature stage, the micropore and mesopore volumes decrease to  $2.84 \text{ cm}^3/\text{kg}$  and  $10.86 \text{ cm}^3/\text{kg}$ , respectively, while the macropore volume increases from  $6.94 \text{ cm}^3/\text{kg}$  to  $13.62 \text{ cm}^3/\text{kg}$ . The BET specific surface area shows a similar pattern to variations in micropore and mesopore volumes. The BET specific surface area values remain relatively stable at low maturity–mature stages before increasing rapidly from  $350 \text{ }^\circ\text{C}$  to  $400 \text{ }^\circ\text{C}$  and subsequently decreasing with increasing temperature.

#### 4.3. FE-SEM observation

FE-SEM observations were made to characterize the pore

structure of each sample at different temperatures (Figs. 5–7).

In the natural sample (S-0), the clay minerals and calcite are interbedded, and microcracks are abundant between the clay minerals (Fig. 5a). The periphery of pyrite grains and some clay minerals are filled with organic matter (Fig. 5b–c). In addition, the organic matter in the natural sample is distributed in strips and irregular blocks, and the internal pores in the organic matter are basically not developed. Some microporous fractures are developed at the contact edge between organic matter and brittle minerals, which may be related to incomplete cementation. The pore type in the gray marl is mainly microcracks.

During the low mature–mature stage, bubble-like organic pores and organic microcracks are obviously developed (Figs. 5 and 6). When the sample enters the oil generation window, kerogen begins to crack and develops round or oval bubble-like pores  $< 1 \mu\text{m}$  in diameter in the organic matter, and shrinkage cracks also develop at the edges of organic matter and minerals (Fig. 5d–f). A few dissolution pores are developed at the edge of the calcite. When the temperature reaches  $330 \text{ }^\circ\text{C}$  ( $R_o = 0.90\%$ ), the internal pores in the

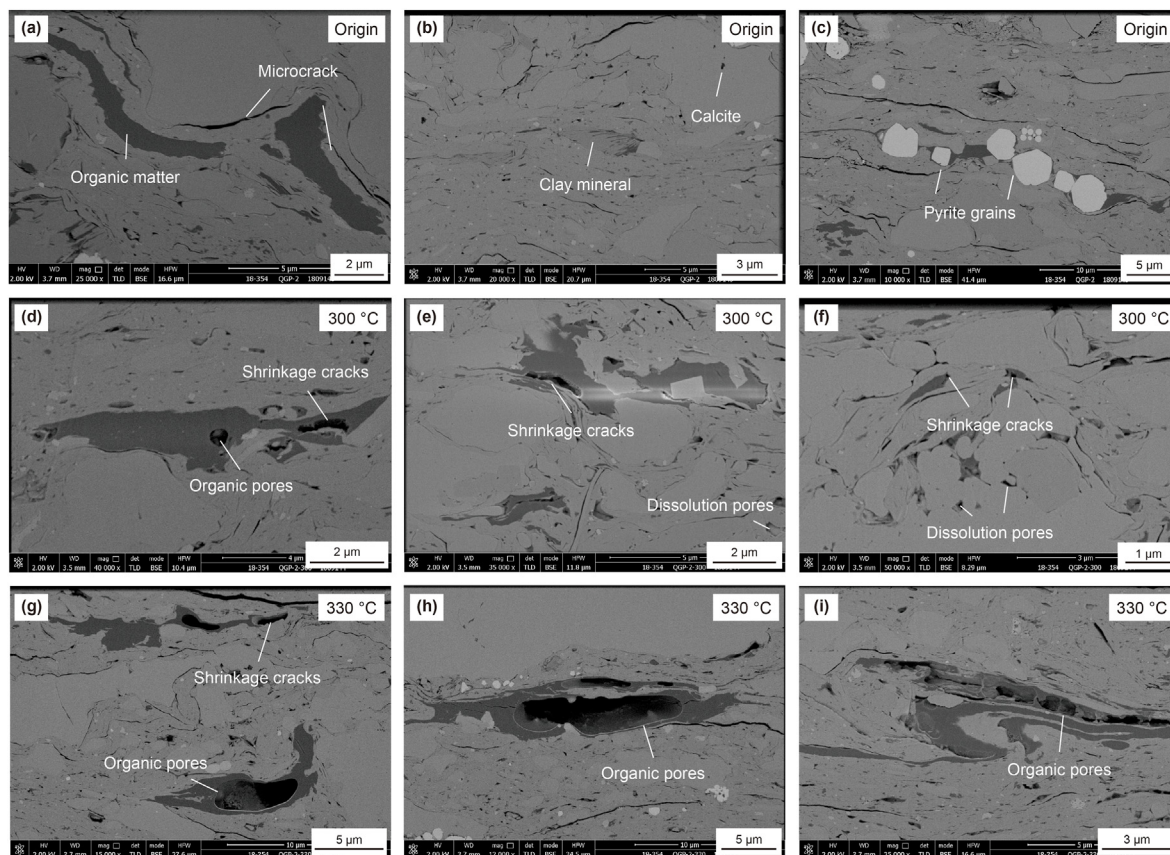


Fig. 5. Pore development characteristics of the simulated gray marl at the low mature–mature stage.

organic matter gradually increase and expand, and the resulting pore size is generally greater than 2  $\mu\text{m}$ . Meanwhile, organic shrinkage cracks develop significantly, and some organic pores with small diameters can be observed between clay mineral layers (Fig. 5g–i). The organic internal pores continue to expand, and several microcracks appear in the organic matter under the influence of static rock pressure (Fig. 6a). The pyrolysis process of some organic matter is sufficient, which results in abundant organic pores in its original position (Fig. 6b). In addition, clay interlayer pores and pyrite intercrystalline pores are well developed in the gray marl (Fig. 6a–c).

During the mature–high mature stage, abundant organic pores and inorganic pores develop, forming a relatively complex nanopore–macropore system. When the temperature reaches 400  $^{\circ}\text{C}$  ( $R_0 = 1.54\%$ ), the internal pores of the organic matter in the gray marl are interconnected to form larger pores or holes, while clay interlayer pores and pyrite intercrystalline pores are also widely developed (Fig. 6d–f). The pore variation characteristics of the gray marl at 425  $^{\circ}\text{C}$  ( $R_0 = 1.72\%$ ) are similar to those at 400  $^{\circ}\text{C}$ . The pores and holes in the organic matter continue to expand, and the distribution area accounts for more than 50% of the initial organic matter area. Clay interlayer pores are well developed, and dissolution pores are sporadically developed on the surface of calcite. In addition, pyrite intercrystalline pores are well developed, and part of the pyrite dissolves to form secondary dissolution pores (Fig. 6g–i).

During the high mature–overmature stage, the easily cracked organic matter is basically consumed, and its internal pores expand to the maximum range. The distribution area of some organic porosity is close to 90% of the initial organic matter area, only some

organic matter remains at the edge, and the hole diameter is generally greater than 5  $\mu\text{m}$  (Fig. 7a–c). In addition, the macropores/holes of organic matter are filled with large calcite and small recrystallized rigid minerals. The clay interlayer pores are also clearly visible. When the temperature is 500  $^{\circ}\text{C}$  ( $R_0 = 2.79\%$ ), there is almost no residual oil in the gray marl during this period. Some of the organic matter surfaces show pores with rounded edges similar to depressions. These internal pores in the organic matter are usually shallow, but the distribution area is relatively large (Fig. 7d). The clay interlayer pores are relatively poorly developed (Fig. 7e). When the temperature is 550  $^{\circ}\text{C}$  ( $R_0 = 3.10\%$ ), the newly formed organic pores in the gas generation stage also begin to expand and interconnect with other pores. At this point, pyrite intergranular pores are well developed (Fig. 7f–i). Clay interlayer pores are well developed during the early overmature stage but poorly developed during the late overmature stage. The pore types in the gray marl are dominated by organic pores, followed by interlayer pores, dissolution pores and intergranular pores.

## 5. Discussion

### 5.1. Correlation between residual oil and porosity in the Mao-1 gray marl

The porosity of gray marl can quantitatively characterize the physical properties of gray marl oil and gas reservoirs (Vik et al., 2013; Bailly et al., 2019). In this paper, the porosities of the samples were measured, and the results show that the evolution of available porosity can be divided into three periods with increasing experimental temperature (Fig. 8). Period I (0–350  $^{\circ}\text{C}$ ) is the period

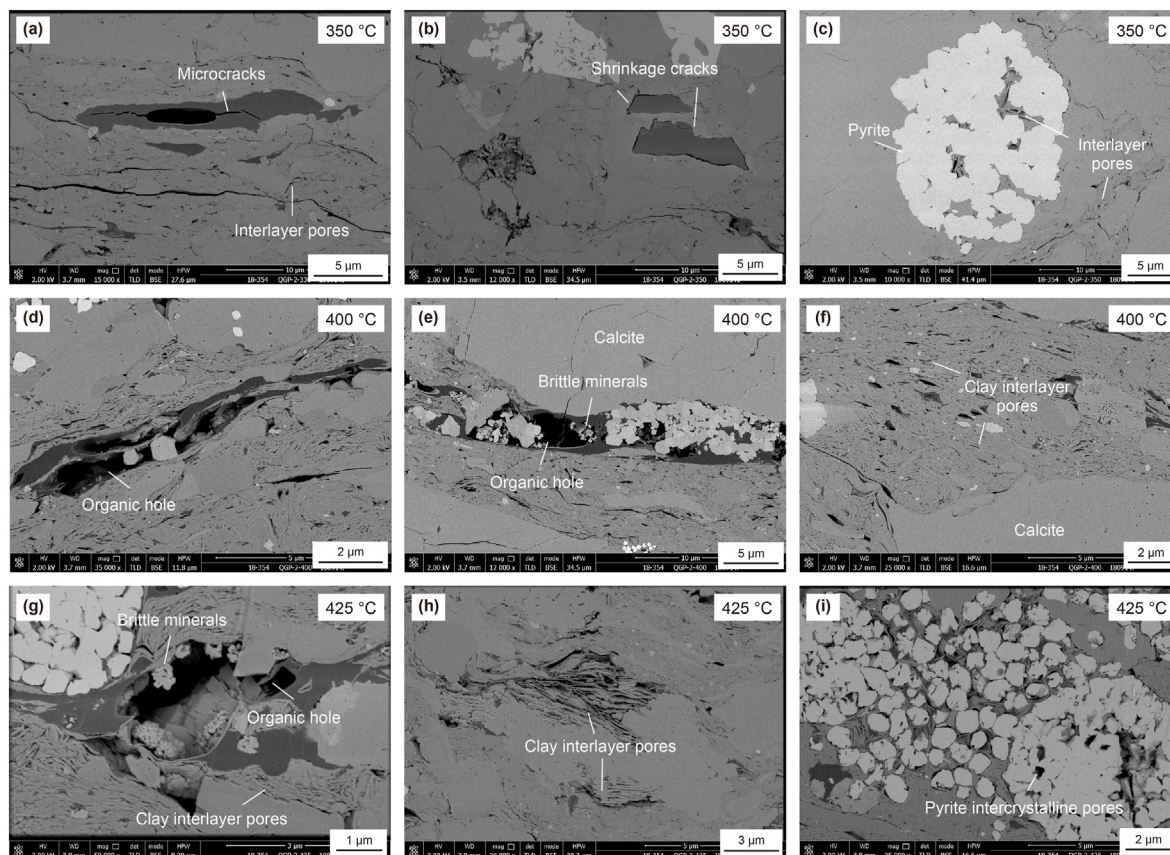


Fig. 6. Pore development characteristics of the simulated gray marl at the mature–high mature stage.

of the rapid decline in the porosity of the gray marl, and the porosity decreases from 8.28% to 5.64%. During this period, the organic matter is at a low mature–mature stage, and kerogen undergoes primary cracking. Although the yield of total oil in the Mao-1 gray marl reaches the generation peak, it is mainly dominated by residual oil or bitumen (Fig. 3a). The large amounts of liquid hydrocarbons and bitumen generated fill the pore space of the gray marl, and only a small amount of crude oil is expelled. The residual oil blocking the primary pores, organic internal pores and organic shrinkage cracks formed in the process of hydrocarbon generation results in an obvious negative correlation between the porosity and the residual oil yield (Fig. 9a).

Period II is the period of the rapid increase in the available porosity of the gray marl, and the porosity ranges from 5.64% to 13.49%, corresponding to the mature–high mature stage (Fig. 8a). During this period, the residual oil yield starts to decline, while the yields of expelled oil and gas increase rapidly (Fig. 3b). The residual oil previously blocked in the marl porosity begins secondary cracking and generates abundant wet gas (Verma et al., 1994; Gong and Gu, 2015; Xiong et al., 2016). The consumption of residual oil releases more pore space, and there is an obvious positive correlation between the porosity and hydrocarbon gas yield in gray marl (Fig. 9b). Period III is the period of a slow increase in porosity from 13.49% to 14.43%, corresponding to the highly mature–overmature stage. The residual oil yield is close to 0 kg/tc, and the expelled oil yield is basically the total oil yield (Fig. 3b). The pore space previously blocked by the residual oil is completely released, while the newly added pore space is mainly produced by the kerogen cracking to gas (Fig. 7). The kerogen consumed in the gas generation stage is much lower than that in the oil generation stage,

resulting in a limited formation of organic pores. In addition, the static rock pressure is also greater than that in the oil generation stage, which may be the reason for the slow increase in porosity in the highly mature–overmature stage.

Many pyrolysis experiments have focused on marine shale and lacustrine shale (Chen et al., 2018b; Guo et al., 2020; Xu et al., 2021a, 2021b), providing ideal opportunity to compare the differences in the porosity evolutions of marl, marine shale, and lacustrine shale obtained from similar pyrolysis experiments. The marine shale data come from the middle Proterozoic Xiamaling shale, with an initial TOC content of 7.18% (Xu et al., 2021b), while the lacustrine shale data come from the Permian Lucaogou shale, with an initial TOC content of 3.1% (Xu et al., 2021a). The porosity trend of lacustrine shale is similar to that of marine shale: the porosity is basically unchanged in the low mature–mature stage and high mature–overmature stage but increases rapidly in the mature–high mature stage (Fig. 8b). By comparing Fig. 8a and b, it can be seen that the generation of residual oil in the low mature–mature stage has little impact on the porosity of marine/lacustrine shale, while the porosity of the gray marl decreases significantly. In addition, although marine and lacustrine shales have a higher TOC content than the Mao-1 Member gray marl, layered bedding is conducive to the discharge of crude oil. The porosity of marine and lacustrine shales at different temperatures is also lower than that of the Mao-1 gray marl, which suggests that more residual oil can accumulate in marl pores than in shale pores. In addition, when the temperature is 400 °C ( $R_o = 1.54\%$ ), the expelled oil yield exceeds the residual oil yield, resulting in rich liquid hydrocarbons accumulating in the gray marl. The organic matter of the Mao-1 natural marl in the Sichuan Basin is generally

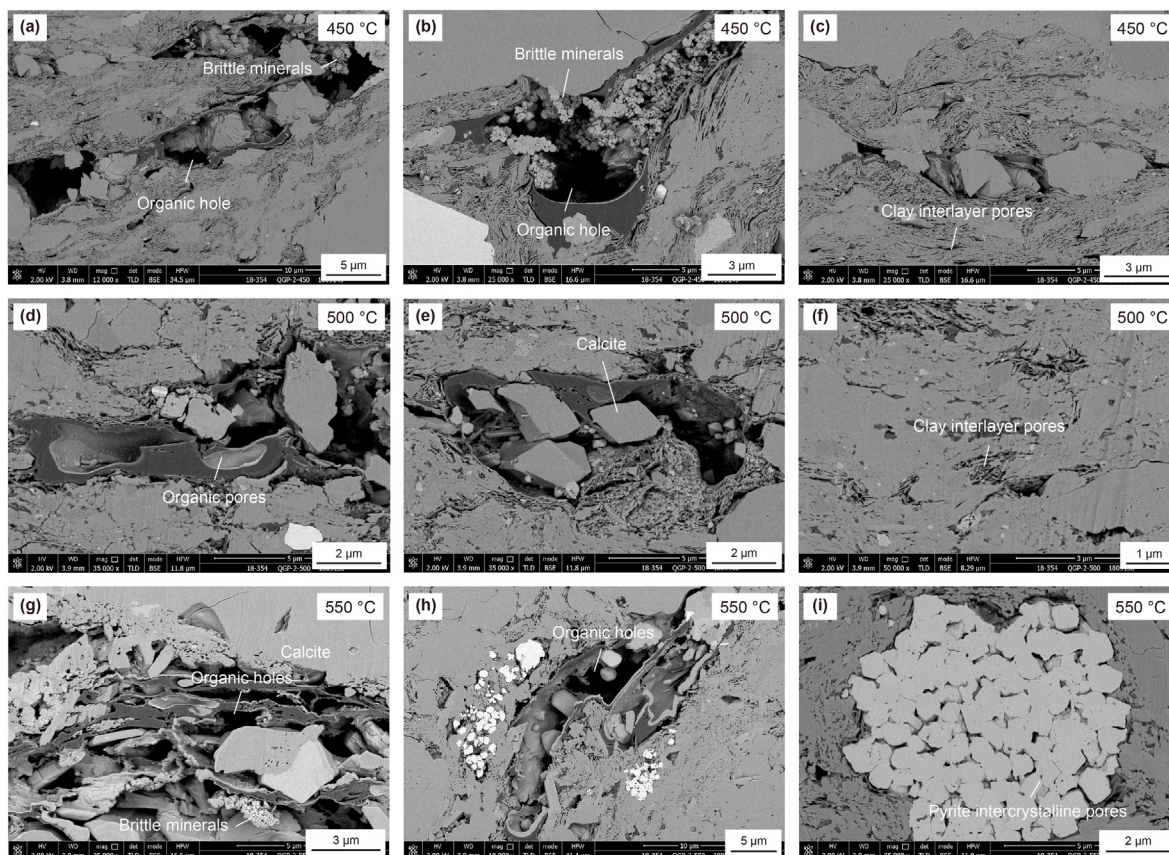


Fig. 7. Pore development characteristics of the simulated gray marl at the high mature–overmature stage.

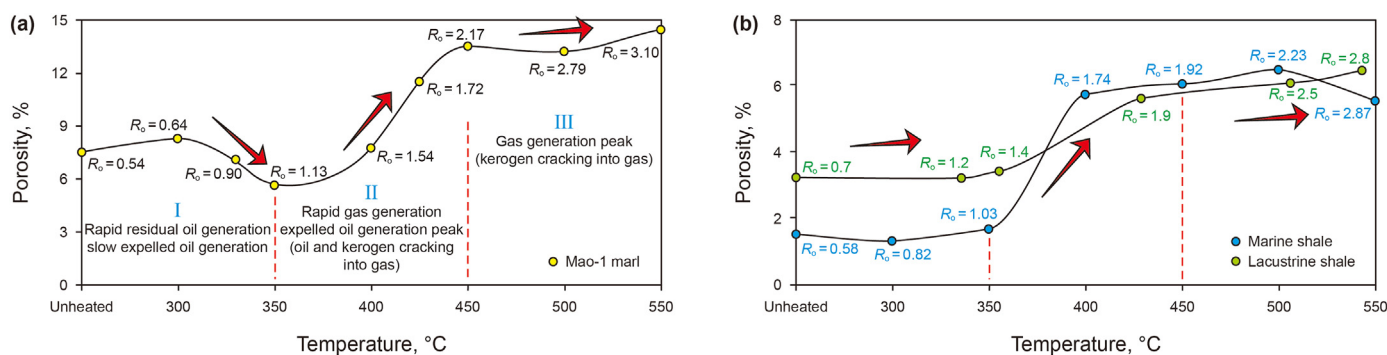


Fig. 8. Porosity variation characteristics of (a) the Permian Mao-1 marl and (b) marine and lacustrine shale with increasing temperature. The lacustrine shale data are from Xu et al. (2021a), and the marine shale data are from Xu et al. (2021b).

at the high mature–overmature stage and is dominated by gas generation. In summary, the massive enrichment of residual oil has laid an important material foundation for the subsequent generation of hydrocarbon gas at the overmaturity stage.

### 5.2. Pore evolution characteristics of gray marl reservoirs

The reservoir characteristics of organic-rich carbonate rocks are of great relevance to unconventional oil and gas resources (Ross and Bustin, 2009). The hydrocarbon generation of organic matter and the transformation of inorganic minerals in gray marl always accompany the diagenetic process and may be the main controlling factors affecting the pore structures.

#### 5.2.1. Variation in pore structure during maturation

The pore types of the gray marl in the low mature–mature stage are mainly organic internal pores and organic shrinkage fractures (Figs. 5 and 6). Notably, the organic internal pores in the Mao-1 gray marl are dominated by macropores, but those in marine/lacustrine shale are mainly mesopores and micropores (Xu et al., 2021b). Why are the pore structures in marl and shale significantly different? Cracking and deacidification of kerogen can produce abundant organic acids and CO<sub>2</sub>, which then combine with water to form acidic fluid. Acidic fluids are more likely to dissolve carbonate minerals in gray marl. However, the SEM observations suggest that carbonate minerals with low organic carbon contents exhibit no obvious dissolution phenomenon and that the dissolution phenomenon mainly occurs in the organic matter. Here, the black

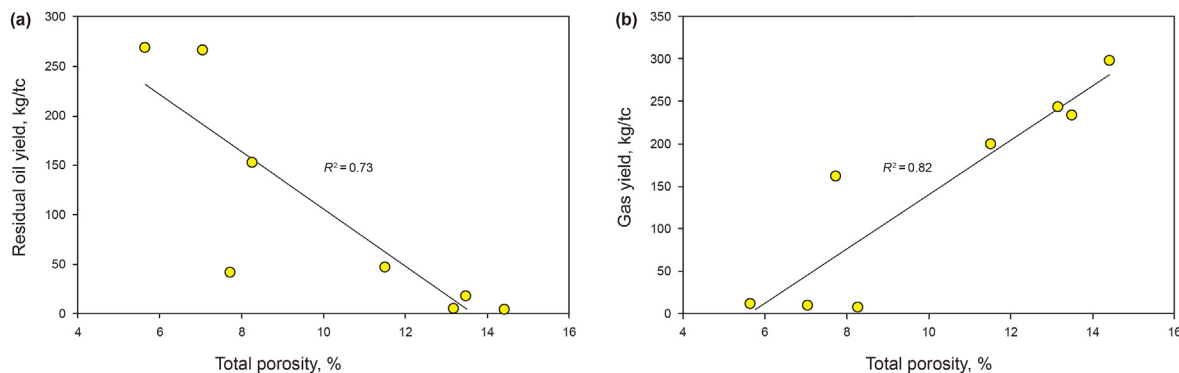


Fig. 9. Correlation between the total porosity and (a) residual oil yield and (b) gas yield.

material in the Mao-1 gray marl (usually named pure organic matter) can be defined as an “organic matter–carbonate mixture” (Figs. 5–7). The acidic fluid generated by kerogen cracking in some carbonates decomposes, resulting in an increase in the CO<sub>2</sub> concentration in the generated gases, and may react with the surrounding carbonate minerals; this process can form relatively large pores in gray marls. Therefore, these pores are both organic pores and dissolution pores. When the experimental temperature is 300–350 °C ( $R_o = 0.9\%–1.13\%$ ), the abundant residual oil or bitumen blocks the organic pores, and the pore volume of macropores is significantly reduced, while the pore volume of micropores and mesopores remain unchanged. According to Fig. 10a–b, the pore size distribution is mainly between 25 and 100 nm at the low mature–mature stage, and the pore types are dominated by mesopores and macropores.

During the mature–high mature stage, the micropore volumes and mesopore volume increase to the maximum value, but the macropore volume decreases to its minimum value first before

increasing gradually (Table 2). The variation in macropore volume should be related to the secondary cracking of residual oil. The release of pore space previously blocked by residual oil results in a change trend of macropore volume that is consistent with that of porosity. SEM observations suggest that there were abundant clay interlayer pores and pyrite intercrystalline pores in the marl at temperatures of 400–450 °C ( $R_o = 1.54\%–2.17\%$ , Figs. 6 and 7). The increase in micropore and mesopore volumes may be related to the transformation of clay minerals, which is mainly characterized by the talcization of sepiolite:



Previous studies have suggested that the clay minerals of the Mao-1 gray marl are mainly sepiolite minerals in northwestern Sichuan ( $R_o < 1.0\%$ ) and talc minerals in southern Sichuan ( $R_o > 1.2\%$ , Tosca and Masterson, 2014; Cai et al., 2019; Su et al., 2020). The talcization of sepiolite usually occurs at the mature–high mature

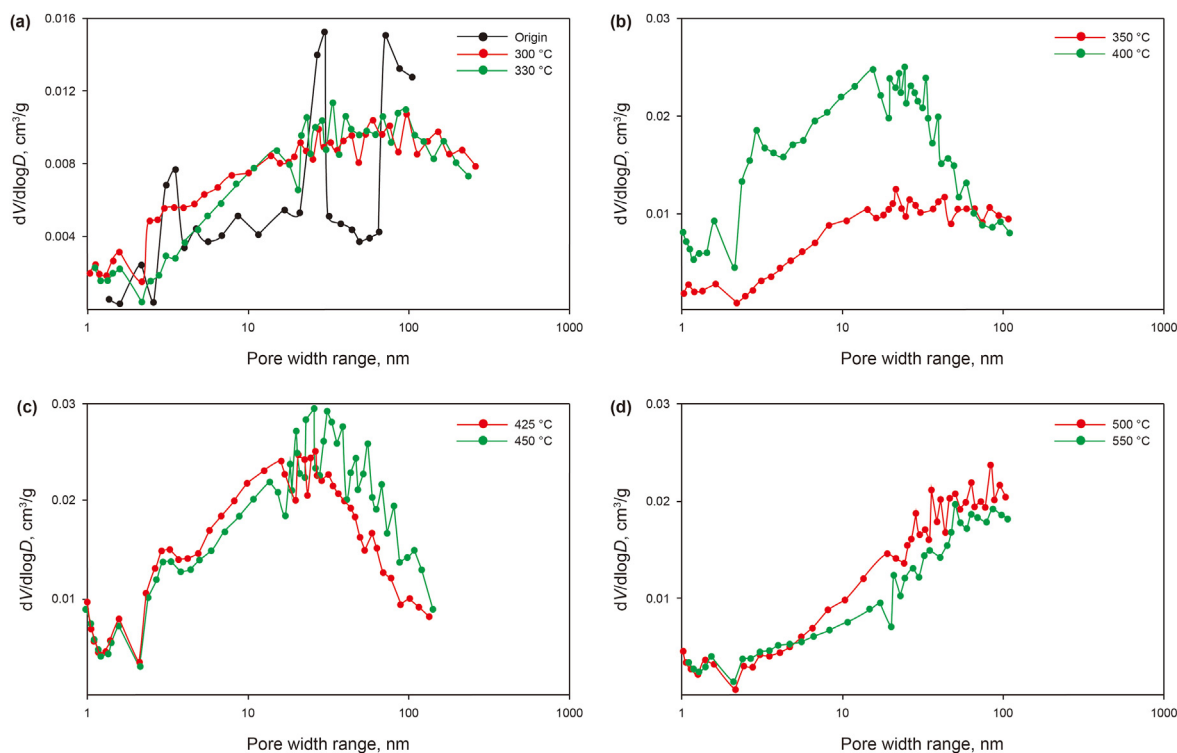


Fig. 10. Pore size distribution curves of the simulated gray marl at different temperatures.

stage of organic matter evolution, which corresponds to the pyrolysis experiments performed at 400–450 °C in this study (Su et al., 2021). There is a small amount of montmorillonite in the Mao-1 marl, which also manifests as the illitization of montmorillonite at this stage. In addition, the acidic environment formed by the process of hydrocarbon generation is conducive to the transformation of clay minerals, which leads to the development of abundant clay interlayer pores. The transformation of clay minerals is also conducive to the cracking of kerogen. Hydrocarbon generation and the transformation of clay minerals are in a mutually promoting coupling process, which jointly increases the pore accessibility of the Mao-1 gray marl. According to Fig. 10c, the pore size distribution shows an obvious single peak, and the pores are mainly mesoporous. The peak value of pore size gradually transitions from 24 nm at 400 °C to 31 nm at 450 °C, indicating a significant increasing trend in the pore structure.

During the high mature–overmature stage, the micropore volume and mesopore volume decrease rapidly or are closed by pyrobitumen, but the macropore volume increases gradually. The transformation of clay minerals basically occurs during this period, and some clay interlayer pores are compacted under the overlying static rock pressure. There were no obvious clay interlayer pores observed in the gray marl at 500–550 °C, which may be one of the main factors controlling the decrease in mesopore volume. However, some rigid mineral particles formed by the transformation of clay minerals develop inside or around the organic matter (Figs. 6 and 7). These mineral particles have strong support and are not easily compacted, which are conducive to the preservation of organic pores. As the hydrocarbon gas yield continues to increase (Fig. 3), some organic pores develop during the overmaturity stage (Fig. 7). The above may be the main controlling factors of the increase in macropore volume in the Mao-1 marl. The pore size distribution curve at 500–550 °C also confirms that the pore size is basically larger than 50 nm and that the macropore volume increases (Fig. 10d).

### 5.2.2. Changes in specific surface area during simulated maturation

The specific surface area is an important factor affecting gas adsorption (and accumulation) in sedimentary rocks. It is generally considered that the specific surface area of pores is positively correlated with the adsorption capacity, which is conducive to the accumulation of natural gas (Ross and Bustin, 2009; Tian et al., 2015). The specific surface area of the gray marl is mainly controlled by the kerogen and clay minerals but is also affected by the kerogen type, maturity, clay mineral type and water content (Zhang et al., 2012; Hao et al., 2013; Tan et al., 2014). In this pyrolysis experiment, the specific surface area decreases slightly at the low mature–mature stage but increases sharply to the maximum value at 400 °C ( $R_o = 1.54\%$ ) and finally decreases at the high mature–overmature stage. The above phenomenon is consistent with the change trend of the total pore volume. Here, the correlations between three pore volumes (the micropore, mesopore, and macropore volumes) and the specific surface area were analyzed.

As shown in Fig. 11, the specific surface area is correlated with micropore volume and mesopore volume but has only a weak correlation with macropore volume. This indicates that the specific surface area is mainly contributed by micropores and mesopores. The higher the proportion of micropores and mesopores is, the larger the specific surface area of the Mao-1 gray marl. The specific surface area of the gray marl is the largest at 400–450 °C ( $R_o = 1.54\text{--}2.17\%$ , Table 2). Therefore, when analyzing the pore types of the samples at these maturities, it is helpful to analyze the relationship between the pore types and specific surface area. When  $R_o$  is 1.54–2.17%, the pores of marl are organic pores, clay

mineral interlayer pores, pyrite intergranular pores and microcracks (Figs. 6 and 7). The size of pores related to organic matter decomposition in gray marl is relatively large and exhibits an obvious macropore type. However, clay interlayer pores and pyrite intergranular pores are usually poorly developed at other maturities. The above results may indicate that clay interlayer pores and pyrite intergranular pores, as typical mesopore types, contribute greatly to the specific surface area, which is conducive to the adsorption of natural gas.

### 5.3. Comparison of pore structure between pyrolysis samples and natural samples

The organic matter of the Mao-1 gray marl in the Sichuan Basin is generally at a highly mature–overmature stage, which is dominated by gas generation (Zhang et al., 2021). In this paper, the pore structures of natural samples and pyrolysis samples are compared to analyze the reliability of the experimental results. The natural sample data were mainly obtained from the JY66-1 well in the Fuling area (Fig. 1). The source rock maturity of the Mao-1 gray marl in the JY66-1 well ranges from 1.71% to 2.18%  $R_o$ , with an average of 1.94% (Hu et al., 2021). In the present study, the samples heated to 425–500 °C ( $R_o = 1.72\text{--}2.79\%$ ) can be compared with the samples from the JY66-1 well to analyze the pore evolution. As shown in Fig. 12, the mesopores with a 10–50 nm pore diameter in the JY66-1 marl provide the main pore volume, followed by the macropores. The pores of the samples heated to 425 °C and 450 °C are also dominated by mesopores, with pore diameters generally ranging from 8 nm to 50 nm, followed by macropores (Fig. 12a–b). The pore structure of the samples is basically consistent with that of natural samples. Furthermore, when the temperature ranges from 425 °C to 500 °C, the proportion of macropores gradually increases, and the pore types are dominated by macropores (Fig. 12c). The mesopores and micropores are closely related to the clay interlayer pores. During the high mature–overmature stage, the dehydration and transformation of clay minerals are gradually weakened, and the residual oil is almost exhausted. Under the action of static rock pressure, the clay interlayer pores are obviously compressed due to the lack of rigid mineral supports. The same trend also appears for the JY66-1 well samples (Fig. 12d). As the burial depth increases, the  $R_o$  value ranges from 1.71% to 2.01%, the proportion of mesopores decreases, and the proportion of macropores gradually increases. The above results show that the pyrolysis experiment can effectively reflect the pore structure evolution of the Mao-1 marl in the process of diagenesis and hydrocarbon generation under natural conditions. The pore type of the Mao-1 marl in the Sichuan Basin is dominated by mesopores in the high mature–overmature stage, and the proportion of macropores increases gradually.

The lithology of the Mao-1 Member is mainly gray marl–limestone rhythmic strata. The TOC content of the gray marl in the JY66-1 well is 0.21–2.41% (average 0.86%), which can be used as an important carbonate source rock (Hu et al., 2021). However, the TOC content of limestone is 0.03–0.43% (average 0.13%), reflecting nearly no hydrocarbon generation capacity. As shown in Figs. 5–7, macropores are mainly developed in the “organic matter–carbonate mineral mixture”. These pores are both organic pores and dissolution pores, which are closely related to the release of organic acids during hydrocarbon generation. However, carbonate minerals with low organic carbon contents basically have no dissolution reaction, which suggests that the Mao-1 limestone with a relatively low porosity and low permeability can act as an important caprock of an unconventional gas reservoir.

In conclusion, abundant residual oil and bitumen may have accumulated in the Mao-1 marl at the low mature–mature stage, which provides a pivotal material foundation for the generation of

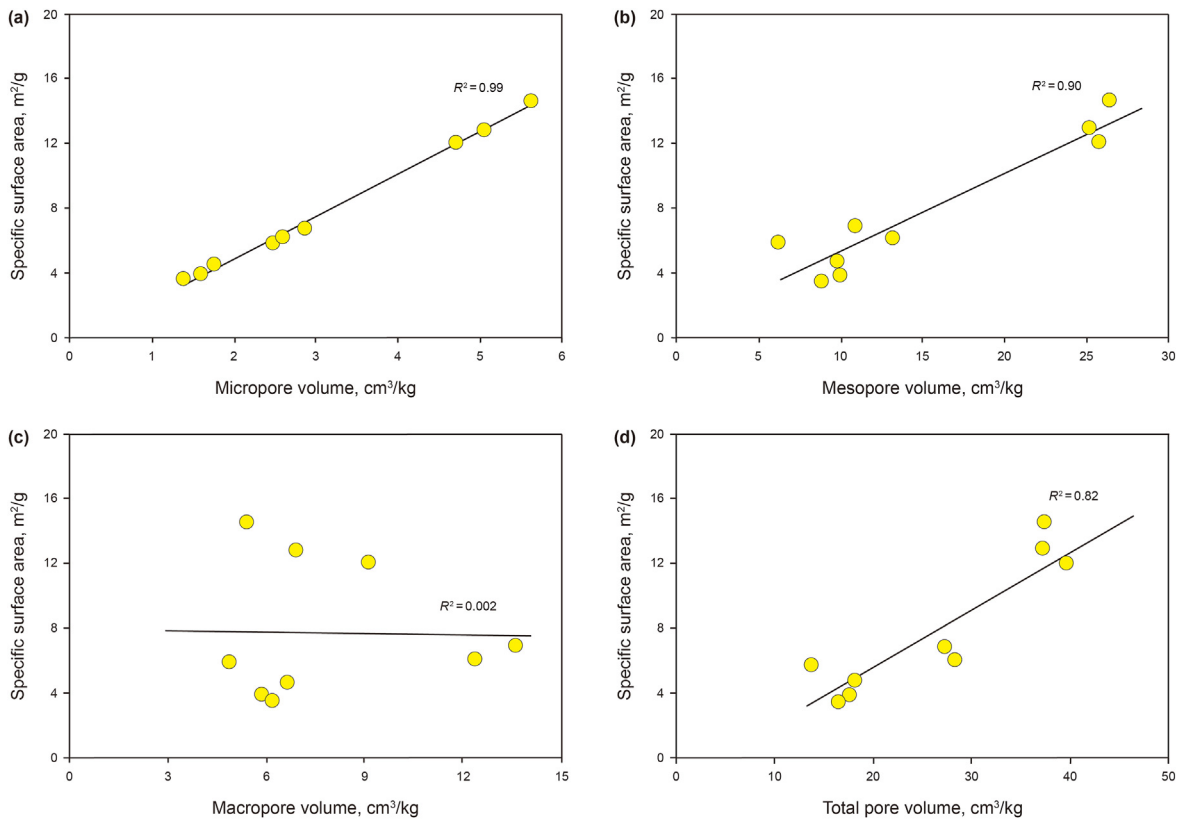


Fig. 11. Correlation between the specific surface area and pore volume.

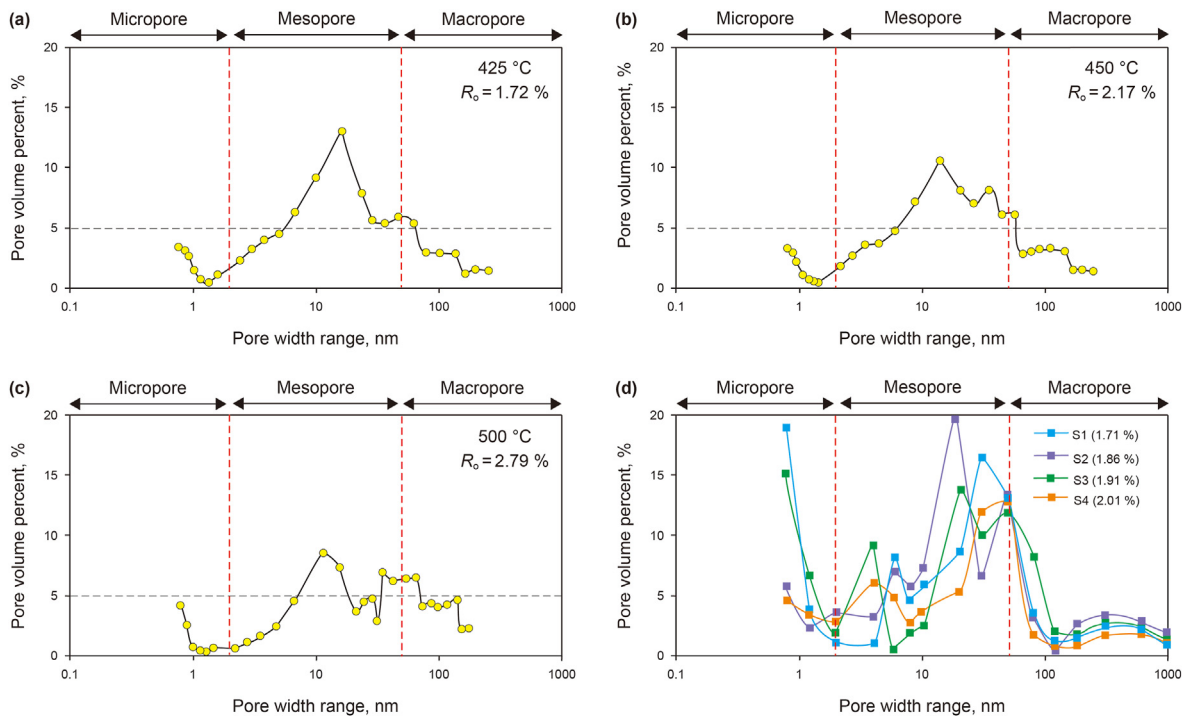


Fig. 12. Pore diameter distributions of the simulated samples at (a) 425 °C, (b) 450 °C, (c) 500 °C, and (d) natural samples of well JY66-1. The data of the JY66-1 samples are modified from Hu et al. (2021).

hydrocarbon gas. Subsequently, the rhythmic strata (marl with well-developed pores and limestone with underdeveloped pores)

constitute an obvious source–storage integrated system during the mature–high mature stage, which ensures the accumulation

conditions for the hydrocarbon gas. This is likely the main reason for oil and gas enrichment in the Maokou Formation in the Sichuan Basin.

5.4. Dynamic evolution model of source–reservoir integration and its geological significance

The pores of the Mao-1 marl are mainly composed of chemically or mechanically generated intergranular pores and microcracks during the early diagenetic stage. In the immature stage ( $R_o < 0.5\%$ ), carbonate minerals were consolidated into rock, the fluid in the formation was discharged rapidly, and the organic matter began to biodegrade and generated little methane gas. Meanwhile, the intergranular pores and microcracks gradually reduced in size under the action of the overlying static rock pressure. The pore evolution of the Mao-1 marl can be divided into the following three stages: the initial pore development stage, rapid pore development stage, and slow pore development stage. The relevant evolution model is shown in Fig. 13.

The initial pore development stage corresponds to the low mature–mature stage. The corresponding  $R_o$  is between 0.54% and 1.13%. Here, the organic matter in Figs. 5–7 can be defined as an “organic matter–carbonate mixture” in the Mao-1 gray marl. Abundant organic acids,  $CO_2$ ,  $H_2S$  and water are discharged during the hydrocarbon generation of organic matter. These acidic fluids are more likely to react and dissolve with surrounding carbonate minerals in the Mao-1 marl, resulting in the formation of relatively large pores. These pores belong to both organic pores and dissolution pores. In addition, carbonate minerals with low organic carbon contents are not dissolved (Fig. 5). As the temperature rises, shrinkage microcracks are formed at the edges of organic matter, but clay minerals basically have no reaction. Although this period is the peak period of oil generation, the oil generated is dominated by residual oil, and little oil is expelled. Abundant liquid hydrocarbons are enriched in the newly formed organic pores and shrinkage microcracks, resulting in an obvious reduction in marl porosity, which is also an important material basis for the formation of carbonate reservoirs.

The rapid pore development stage corresponds to the

mature–high mature stage, in which  $R_o$  is between 1.13% and 1.72%. The residual oil in the gray marl begins to crack into condensate oil and moisture, which may increase the pore fluid pressure. The pores and microcracks previously blocked by the residual oil and bitumen are released, and the available porosity of the Mao-1 marl increases rapidly. In addition, this period is also in the middle to late diagenetic stage, when sepiolite begins to transform into allietite and talc and releases some rigid mineral  $SiO_2$  (Fig. 13). There is also a small amount of montmorillonite, which is dehydrated and transformed into illite. The transformation of clay minerals is also conducive to the cracking of kerogen. The acidic environment formed by the process of hydrocarbon generation is conducive to the transformation of clay minerals. Hydrocarbon generation and the transformation of clay minerals are in a mutually promoting coupling process, which jointly promotes the pore accessibility of the Mao-1 gray marl. The dehydration and transformation of clay minerals contribute considerable mesopore and micropore volumes. The newly formed rigid mineral  $SiO_2$  is beneficial to the preservation of organic pores (Fig. 6e–g). During the early stage of high maturity (350–400 °C,  $R_o = 1.13\%–1.54\%$ ), the gas generation mechanism was dominated by the cracking of residual oil (Fig. 13). Therefore, the pore type is mainly mesopores, followed by micropores and macropores. When the temperature exceeds 425 °C ( $R_o = 1.72\%$ ), the residual oil is fully consumed, and the generation of hydrocarbon gas mainly depends on the secondary cracking of organic matter. The contribution of macropores in the Mao-1 marl increases gradually, which is close to the mesopore proportion.

Notably, the porosity of marl decreases slightly at 450–500 °C ( $R_o = 2.17–2.79\%$ ), while the micropore volume and mesopore volume decrease significantly (Fig. 13). The dehydration and transformation processes of clay minerals basically end in this period. The above phenomenon should be the result of pore compression caused by the overlying static rock pressure. Contrastingly, the majority of organic matter is filled between rigid minerals and is less affected by compaction pressure (Fig. 7). The organic matter is still in secondary cracking gas stage. As a result, this type pores filled in the organic matter slowly increase, expand and partially interconnected, which leads to the continuous growth of macropore volume. When the temperature is 500–550 °C

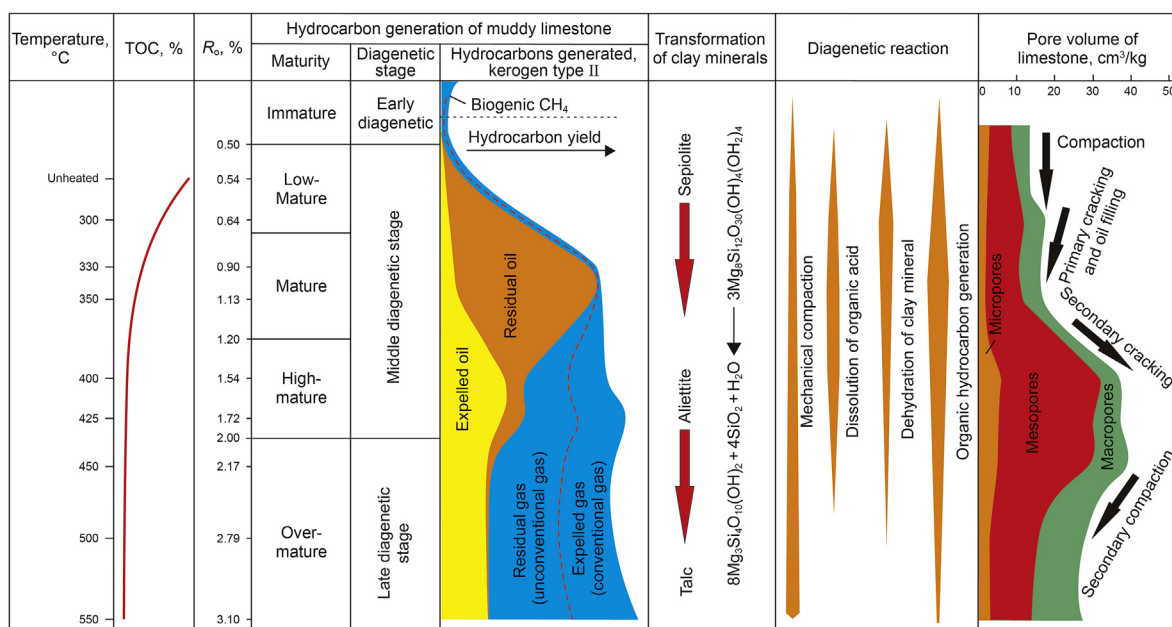


Fig. 13. Pore evolution model and hydrocarbon generation based on the pyrolysis experiments in organic-rich carbonate rock.

( $R_o = 2.79\text{--}3.10\%$ ), corresponding to the high maturity stage, the pore evolution of the Mao-1 marl is characterized by a slow development stage. The methane gas yield gradually increases, and a small amount of liquid oil is expelled (Fig. 13). Fig. 7 shows that the pores in the organic matter formed a more complex pore network system, which is conducive to the enrichment of natural gas. Meanwhile, due to the further enhancement of compaction action, some original pores should be destroyed, and the development of organic pores is also limited (Tian et al., 2015). The whole pore system basically maintains a relatively stable state.

The Mao-1 gray marl–limestone rhythmic strata are a newly recognized formation of unconventional gas reservoirs with source–reservoir integration. As shown in Fig. 13,  $R_o$  is 1.7–2.5% in the Mao-1 marl, and hydrocarbon generation and reservoir configuration are the best in this range, as is the gas reservoir potential. After  $R_o > 2.5\%$ , the pore space is compressed or closed by pyrobitumen, and the residual oil has been consumed completely, which may be unfavorable to the enrichment of natural gas. In addition, several layers of organic-rich carbonate rock similar to the Mao-1 gray marl were developed in South China, i.e., the Triassic Leikoupo Formation, Permian Qixia Formation, Wujiaping Formation, and Longtan Formation (Chen, 2009; Luo et al., 2014; He et al., 2019). The above strata are dominated by carbonate platforms or carbonate slope facies. The TOC content of limestone is generally greater than 0.8%, and the organic matter is at the high mature–overmature stage, which indicates good exploration potential. Combined with the characteristics of the Mao-1 gas reservoir, three important considerations for finding similar oil and gas reservoirs are (1) a high TOC content, (2) marl gas generation capacity and reservoir  $R_o$  of 1.7%–2.5%, and (3) clear identification of the top and bottom boundaries. In summary, the dynamic evolution characteristics of the source–reservoir integration of the Mao-1 gray marl can provide a scientific basis and evaluation parameters for the exploration and development of unconventional carbonate gas reservoirs.

## 6. Conclusions

Through a semiclosed pyrolysis experiment on organic-rich marl samples, this paper analyzed the formation and evolution of pores from low maturity to overmaturity. The results revealed that the pore size of marl is widely distributed over a range of temperatures and that the pore types are mainly mesopores and macropores. Due to the effect of pores blocked by residual oil, the available porosity of marl has a clear trend of first decreasing and then increasing with increasing temperature. In addition, some large organic internal pores and shrinkage microcracks are developed in organic matter–carbonate mineral mixtures during the hydrocarbon generation process, while carbonate minerals with low organic carbon contents basically do not dissolve and thus do not form dissolution pores. These organic internal pores gradually expand and interconnect to form larger macropores or holes, which is the main pore type of the Mao-1 marl at the overmaturity stage. The micropores and mesopores mainly develop at the high mature–overmature stage and are dominated by clay mineral interlayer pores and pyrite intergranular pores. The transformation of clay minerals is characterized by the talcization process of sepiolite at the middle diagenetic stage and forms micropores and mesopores in the gray marl. Micropores and mesopores are the main contributors to the specific surface area, which is conducive to natural gas adsorption. However, due to the weakening of clay mineral transformation and the enhancement of compaction, the micropore and mesopore volumes are obviously compressed at the overmaturity stage. Kerogen continues to produce methane gas, and some new organic pores are developed. The whole pore system

of this marl remains relatively stable.

In summary, abundant residual oil accumulates at the low mature–mature stage and provides a pivotal material foundation for the generation of hydrocarbon gas. Subsequently, the rhythmic strata constitute an obvious source–storage integrated system and ensure the accumulation conditions for hydrocarbon gas, which may be the main reason for the oil and gas enrichment in the Maokou Formation in the Sichuan Basin.

## Acknowledgments

This work was supported by the National Natural Science Foundation of China (42072156; U19B6003); and the Open Foundation of Cooperative Innovation Center of Unconventional Oil and Gas, Yangtze University, China (No. UOG2022-18). We thank two anonymous reviewers for constructive comments on earlier versions of the manuscript.

## References

- Bai, L., Liu, B., Du, Y., et al., 2022. Distribution characteristics and oil mobility thresholds in lacustrine shale reservoir: insights from  $N_2$  adsorption experiments on samples prior to and following hydrocarbon extraction. *Petrol. Sci.* 19 (2), 486–497. <https://doi.org/10.1016/j.petsci.2021.10.018>.
- Bailly, C., Adelinet, M., Hamon, Y., et al., 2019. Combined controls of sedimentology and diagenesis on seismic properties in lacustrine and palustrine carbonates (Upper Miocene, Samos Island, Greece). *Geophys. J. Int.* 219 (2), 1300–1315. <https://doi.org/10.1093/gji/ggz365>.
- Brunauer, S., Deming, L.S., Deming, W.E., et al., 1940. On a theory of the van der Waals adsorption of gases. *J. Am. Chem. Soc.* 62 (7), 1723–1732. <https://doi.org/10.1021/ja01864a025>.
- Cai, Z., Li, J., Chen, H., et al., 2019. Genesis of Mg-phyllosilicate occurrences in the middle permian marine successions of South China. *Appl. Clay Sci.* 181 (15), 105242. <https://doi.org/10.1016/j.clay.2019.105242>.
- Chen, G., Lin, J., Hu, W., et al., 2018a. Characteristics of a crude oil composition and its in situ waxing inhibition behavior. *Fuel* 218 (15), 213–217. <https://doi.org/10.1016/j.fuel.2017.12.116>.
- Chen, S., Zuo, Z., Moore, T.A., et al., 2018b. Nanoscale pore changes in a marine shale: a case study using pyrolysis experiments and nitrogen adsorption. *Energy Fuel* 32 (9), 9020–9032. <https://doi.org/10.1021/acs.energyfuels.8b01405>.
- Chen, Z., 2009. Discussion on gas exploration of middle permian Qixia Formation, Sichuan Basin. *Nat. Gas Geosci.* 20 (3), 325–334. <https://doi.org/10.11764/j.issn.1672-1926.2009.03.325> (In Chinese).
- Chen, Z., Guo, Q., Jiang, C., et al., 2017. Source rock characteristics and rock-eval-based hydrocarbon generation kinetic models of the lacustrine Chang-7 shale of Triassic Yanchang formation, Ordos basin, China. *Int. J. Coal Geol.* 182, 52–65. <https://doi.org/10.1016/j.coal.2017.08.017>.
- Curtis, J.B., 2002. Fractured shale-gas systems. *AAPG Bull.* 86 (11), 1921–1938. <https://doi.org/10.1306/61EEDDBE-173E-11D7-8645000102C1865D>.
- Garcia, B., Pinkston, D., Loucks, R.G., et al., 2018. The Three Forks playa lake depositional model: implications for characterization and development of an unconventional carbonate play. *AAPG Bull.* 102 (8), 1455–1488. <https://doi.org/10.1306/12081716510>.
- Gong, Y., Gu, Y., 2015. Experimental study of water and  $CO_2$  flooding in the tight main pay zone and vuggy residual oil zone of a carbonate reservoir. *Energy Fuel* 29 (10), 6213–6223. <https://doi.org/10.1021/acs.energyfuels.5b01185>.
- Gregg, S.J., Sing, K.S.W., Salzberg, H., 1967. Adsorption surface area and porosity. *J. Electrochem. Soc.* 114 (11), 279C. <https://doi.org/10.1002/ebpp.19670710837>.
- Guo, H., Jia, W., He, R., et al., 2020. Distinct evolution trends of nanometer-scale pores displayed by the pyrolysis of organic matter-rich lacustrine shales: implications for the pore development mechanisms. *Mar. Petrol. Geol.* 121, 104622. <https://doi.org/10.1016/j.marpetgeo.2020.104622>.
- Guo, H., Jia, W., Peng, P., et al., 2017. Evolution of organic matter and nanometer-scale pores in an artificially matured shale undergoing two distinct types of pyrolysis: a study of the Yanchang shale with type II kerogen. *Org. Geochem.* 105, 56–66. <https://doi.org/10.1016/j.orggeochem.2017.01.004>.
- Hao, F., Zou, H., Lu, Y., 2013. Mechanisms of shale gas storage: implications for shale gas exploration in China. *AAPG Bull.* 97 (8), 1325–1346. <https://doi.org/10.1306/02141312091>.
- He, D., Ma, Y., Li, Y., et al., 2019. New directions in an established gas play: promising dolomite reservoirs in the middle triassic Leikoupo Formation of the Sichuan Basin, China. *AAPG Bull.* 103 (1), 1–29. <https://doi.org/10.1306/05111816502>.
- Hu, D., Wang, L., Zhang, H., et al., 2021. Discovery of carbonate source rock gas reservoir and its petroleum geological implications: a case study of the gas reservoir in the first member of Middle Permian Maokou formation in the Fuling area, Sichuan basin. *Nat. Gas. Ind. B.* 8 (1), 13–23. <https://doi.org/10.1016/j.ngib.2020.07.001> (In Chinese).
- Jarvie, D.M., Hill, R.J., Ruble, T.E., et al., 2007. Unconventional shale-gas systems: the Mississippian Barnett shale of North-Central Texas as one model for

- thermogenic shale-gas assessment. *AAPG Bull.* 91 (4), 475–499. <https://doi.org/10.1306/12190606068>.
- Jia, D., Wei, G., Chen, Z., et al., 2006. Longmen Shan fold-thrust belt and its relation to the Western Sichuan basin in Central China: new insights from hydrocarbon exploration. *AAPG Bull.* 90 (9), 1425–1447. <https://doi.org/10.1306/03230605076>.
- Klaver, J., Desbois, G., Littke, R., et al., 2015. BIB-SEM characterization of pore space morphology and distribution in postmature to overmature samples from the Haynesville and Bossier shales. *Mar. Petrol. Geol.* 59, 451–466. <https://doi.org/10.1016/j.marpetgeo.2014.09.020>.
- Ko, L.T., Loucks, R.G., Zhang, T., et al., 2016. Pore and pore network evolution of upper cretaceous boquillas (eagle ford—equivalent) mudrocks: results from gold tube pyrolysis experiments. *AAPG Bull.* 100 (11), 1693–1722. <https://doi.org/10.1306/04151615092>.
- Kuang, L., Hou, L., Wu, S., et al., 2022. Organic matter occurrence and pore-forming mechanisms in lacustrine shales in China. *Petrol. Sci.* 19 (4), 1460–1472. <https://doi.org/10.1016/j.petsci.2022.03.005>.
- Lewan, M.D., Roy, S., 2011. Role of water in hydrocarbon generation from Type-I kerogen in Mahogany oil shale of the Green River Formation. *Org. Geochem.* 42 (1), 31–41. <https://doi.org/10.1016/j.orggeochem.2010.10.004>.
- Lei, Y., Luo, X., Wang, X., et al., 2015. Characteristics of silty laminae in Zhangjiatan shale of Southeastern Ordos basin, China: implications for shale gas formation. *AAPG Bull.* 99 (4), 661–687. <https://doi.org/10.1306/09301414059>.
- Li, A., Shan, X., Luo, K., et al., 2021a. A new type of unconventional gas reservoir from the nodular limestones of the Middle Permian Maokou formation in the South-Eastern Sichuan basin, South-West China. *Geol. J.* 56 (11), 5426–5439. <https://doi.org/10.1002/gj.4250>.
- Li, F., Wang, M., Liu, S., et al., 2019a. Pore characteristics and influencing factors of different types of shales. *Mar. Petrol. Geol.* 102, 391–401. <https://doi.org/10.1016/j.marpetgeo.2018.11.034>.
- Li, H., Tang, H., Qin, Q., et al., 2019b. Characteristics, formation periods and genetic mechanisms of tectonic fractures in the tight gas sandstones reservoir: a case study of Xujiatahe formation in YB area, Sichuan basin, China. *J. Pet. Sci. Eng.* 178, 723–735. <https://doi.org/10.1016/j.petrol.2019.04.007>.
- Li, H., Xie, X., Huang, J., et al., 2012. Main factors controlling the formation of excellent marine source rocks in Permian Maokou formation of Northwest Sichuan, China. *Earth Sci. J. China Univ. Geosci.* 37, 171–180. <https://doi.org/10.3777/dqkx.2012.017>. (In Chinese).
- Li, Y., Kang, Z., Xue, Z., et al., 2018. Theories and practices of carbonate reservoirs development in China. *Petrol. Explor. Dev.* 45 (4), 712–722. [https://doi.org/10.1016/S1876-3804\(18\)30074-0](https://doi.org/10.1016/S1876-3804(18)30074-0).
- Li, Y., Xu, F., Zeng, L., et al., 2021b. Gas source in lower Permian Maokou formation and gas accumulation in the syncline area of Eastern Sichuan basin. *J. Pet. Sci. Eng.* 206, 109044. <https://doi.org/10.1016/j.petrol.2021.109044>.
- Liu, K., Wang, L., Ostadhassan, M., et al., 2019. Nanopore structure comparison between shale oil and shale gas: examples from the Bakken and Longmaxi Formations. *Petrol. Sci.* 16, 77–93. <https://doi.org/10.1007/s12182-018-0277-3>.
- Liu, R., Luo, B., Li, Y., et al., 2021. Relationship between Permian volcanic rocks distribution and karst paleogeomorphology of Maokou formation and its significance for petroleum exploration in Western Sichuan basin, SW China. *Petrol. Explor. Dev.* 48 (3), 670–682. [https://doi.org/10.1016/S1876-3804\(21\)60053-8](https://doi.org/10.1016/S1876-3804(21)60053-8).
- Liu, W., Liu, J., Cai, M., et al., 2017. Pore evolution characteristic of shale in the Longmaxi formation, Sichuan basin. *Pet. Res.* 2 (4), 291–300. <https://doi.org/10.1016/j.ptlrs.2017.03.003>.
- Liu, X., Guan, M., Jin, Z., et al., 2022. Pore structure evolution of lacustrine organic-rich shale from the second member of the Kongdian formation in the Cangdong Sag, Bohai Bay Basin, China. *Petrol. Sci.* 19 (2), 459–471. <https://doi.org/10.1016/j.petsci.2021.12.010>.
- Lønøy, A., 2006. Making sense of carbonate pore systems. *AAPG Bull.* 90 (9), 1381–1405. <https://doi.org/10.1306/03130605104>.
- Lucia, F., 1983. Petrophysical parameters estimated from visual descriptions of carbonate rocks: a field classification of carbonate pore space, 03 J. *Petrol. Technol.* 35, 629–637. <https://doi.org/10.2118/10073-PA>.
- Luo, J., He, Y., Wang, R., et al., 2014. Lithofacies palaeogeography of the late permian wujiaping age in the middle and upper Yangtze region, China. *J. Palaeogeogr.* 3 (4), 384–409. <https://doi.org/10.3724/SP.J.1261.2014.00063>.
- Ma, Y., Cai, X., Zhao, P., 2018. China's shale gas exploration and development: understanding and practice. *Petrol. Explor. Dev.* 45 (4), 589–603. [https://doi.org/10.1016/S1876-3804\(18\)30065-X](https://doi.org/10.1016/S1876-3804(18)30065-X).
- Ma, Y., He, D., Cai, X., et al., 2017. Distribution and fundamental science questions for petroleum geology of marine carbonate in China. *Acta Petrol. Sin.* 33 (4), 1007–1020. (In Chinese).
- Ma, Z., Tan, J., Zheng, L., et al., 2021. Evaluating gas generation and preservation of the Wufeng-Longmaxi Formation shale in southeastern Sichuan Basin, China: implications from semiclosed hydrous pyrolysis. *Mar. Petrol. Geol.* 129, 105102. <https://doi.org/10.1016/j.marpetgeo.2021.105102>.
- Mastalerz, M., Schimmelmann, A., Drobnik, A., et al., 2013. Porosity of devonian and mississippian New Albany shale across a maturation gradient: insights from organic petrology, gas adsorption, and mercury intrusion geohorizon. *AAPG Bull.* 97 (10), 1621–1643. <https://doi.org/10.1306/04011312194>.
- Pommer, M., Milliken, K., 2015. Pore types and pore-size distributions across thermal maturity, eagle ford formation, Southern Texas. *AAPG Bull.* 99 (9), 1713–1744. <https://doi.org/10.1306/03051514151>.
- Radwan, A.E., Trippetta, F., Kassem, A., et al., 2021. Multi-scale characterization of unconventional tight carbonate reservoir: insights from October oil field, Gulf of Suez rift basin, Egypt. *J. Pet. Sci. Eng.* 197, 107968. <https://doi.org/10.1016/j.petrol.2020.107968>.
- Ross, D.J., Bustin, R.M., 2009. The importance of shale composition and pore structure upon gas storage potential of shale gas reservoirs. *Mar. Petrol. Geol.* 26 (6), 916–927. <https://doi.org/10.1016/j.marpetgeo.2008.06.004>.
- Ross, D.J., Bustin, R.M., 2007. Shale gas potential of the lower jurassic gordondale member, Northeastern British Columbia, Canada. *Bull. Can. Petrol. Geol.* 55 (1), 51–75. <https://doi.org/10.2113/gscpgbull.55.1.51>.
- Schieber, J., 2010. Common themes in the formation and preservation of intrinsic porosity in shales and mudstones—illustrated with examples across the phanerozoic, SPE Unconventional Gas Conference. *OnePetro*, SPE-132370-MS. <https://doi.org/10.2118/132370-MS>.
- Sing, K.S., 1985. Reporting physisorption data for gas/solid systems with special reference to the determination of surface area and porosity (recommendations 1984). *Pure Appl. Chem.* 57 (4), 603–619. <https://doi.org/10.1351/pac198557040603>.
- Song, Y., Li, Z., Jiang, L., et al., 2015. The concept and the accumulation characteristics of unconventional hydrocarbon resources. *Petrol. Sci.* 12 (4), 563–572. <https://doi.org/10.1007/s12182-015-0060-7>.
- Su, C., Li, F., Tan, X., et al., 2020. Recognition of diagenetic contribution to the formation of limestone-marl alternations: a case study from Permian of South China. *Mar. Petrol. Geol.* 111, 765–785. <https://doi.org/10.1016/j.marpetgeo.2019.08.033>.
- Su, C., Li, R., Shi, G., et al., 2021. Reservoir characteristics of the first member of Middle Permian Maokou formation in Sichuan basin and its periphery and inspirations to oil and gas exploration. *Petrol. Explor. Dev.* 48 (6), 1–12. [https://doi.org/10.1016/S1876-3804\(21\)60290-2](https://doi.org/10.1016/S1876-3804(21)60290-2).
- Su, W., Jiang, Q., Chen, Z., et al., 2015. Sequence stratigraphic features of the Middle Permian Maokou formation in the Sichuan basin and their controls on source rocks and reservoirs. *Nat. Gas. Ind. B.* 2 (5), 421–429. <https://doi.org/10.1016/j.ngib.2015.09.018>. (In Chinese).
- Sun, M., Yu, B., Hu, Q., et al., 2017. Pore characteristics of Longmaxi shale gas reservoir in the Northwest of Guizhou, China: investigations using small-angle neutron scattering (SANS), helium pycnometry, and gas sorption isotherm. *Int. J. Coal Geol.* 171, 61–68. <https://doi.org/10.1016/j.coal.2016.12.004>.
- Tan, J., Weniger, P., Krooss, B., et al., 2014. Shale gas potential of the major marine shale formations in the Upper Yangtze platform, South China, part II: methane sorption capacity. *Fuel* 129, 204–218. <https://doi.org/10.1016/j.fuel.2014.03.064>.
- Tang, D., Xiao, D., Tan, X., et al., 2016. Restoration of paleokarst landform and its geological significance: a case from Middle Permian Maokou formation in Northwestern Sichuan basin. *Petrol. Explor. Dev.* 43 (5), 751–758. [https://doi.org/10.1016/S1876-3804\(16\)30090-8](https://doi.org/10.1016/S1876-3804(16)30090-8).
- Tang, Y., Cao, J., He, W., et al., 2021. Discovery of shale oil in alkaline lacustrine basins: the late paleozoic fengcheng formation, mahu sag, junggar basin, China. *Petrol. Sci.* 18 (5), 1281–1293. <https://doi.org/10.1016/j.petsci.2021.04.001>.
- Tian, H., Pan, L., Zhang, T., et al., 2015. Pore characterization of organic-rich lower cambrian shales in Qiannan depression of Guizhou province, Southwestern China. *Mar. Petrol. Geol.* 62, 28–43. <https://doi.org/10.1016/j.marpetgeo.2015.01.004>.
- Topór, T., Derkowski, A., Ziemiński, P., et al., 2017. The effect of organic matter maturation and porosity evolution on methane storage potential in the Baltic basin (Poland) shale-gas reservoir. *Int. J. Coal Geol.* 180, 46–56. <https://doi.org/10.1016/j.coal.2017.07.005>.
- Tosca, N., Masterson, A., 2014. Chemical controls on incipient Mg-silicate crystallization at 25°C: implications for early and late diagenesis. *Clay Miner.* 49 (2), 165–194. <https://doi.org/10.1180/claymin.2014.049.2.03>.
- Valentine, B.J., Hackley, P.C., Hatcherian, J.J., 2021. Hydrous pyrolysis of New Albany Shale: a study examining maturation changes and porosity development. *Mar. Petrol. Geol.* 134, 105368. <https://doi.org/10.1016/j.marpetgeo.2021.105368>.
- Verma, M.K., Boucherit, M., Bouvier, L., 1994. Evaluation of residual oil saturation after waterflood in a carbonate reservoir, 04 SPE Reservoir Eng. 9, 247–253. <https://doi.org/10.2118/21371-PA>.
- Verwer, K., Eberli, G.P., Weger, R.J., 2011. Effect of pore structure on electrical resistivity in carbonates. *AAPG Bull.* 95 (2), 175–190. <https://doi.org/10.1306/06301010047>.
- Vik, B., Bastesen, E., Skauge, A., 2013. Evaluation of representative elementary volume for a vuggy carbonate rock—part: porosity, permeability, and dispersivity. *J. Pet. Sci. Eng.* 112, 36–47. <https://doi.org/10.1016/j.petrol.2013.03.029>.
- Wang, F., Guo, S., 2019. Influential factors and model of shale pore evolution: a case study of a continental shale from the Ordos basin. *Mar. Petrol. Geol.* 102, 271–282. <https://doi.org/10.1016/j.marpetgeo.2018.12.045>.
- Wang, Z., Tan, J., Boyle, R., et al., 2020. Evaluating episodic hydrothermal activity in South China during the early Cambrian: implications for biotic evolution. *Mar. Petrol. Geol.* 117, 104355. <https://doi.org/10.1016/j.marpetgeo.2020.104355>.
- Wang, J., Guo, S., 2021. Study on the relationship between hydrocarbon generation and pore evolution in continental shale from the Ordos Basin, China. *Petrol. Sci.* 18 (5), 1305–1322. <https://doi.org/10.1016/j.petsci.2021.01.002>.
- Wei, G., Yang, W., Zhu, Y., et al., 2010. Depositional system of the middle permian Qixia Formation in the western Sichuan Basin. *Oil Gas Geol.* 31 (4), 442–448. <https://doi.org/10.11743/ogg20100407>. (In Chinese).
- Xiong, F., Jiang, Z., Chen, J., et al., 2016. The role of the residual bitumen in the gas storage capacity of mature lacustrine shale: a case study of the Triassic Yan-chang shale, Ordos basin, China. *Mar. Petrol. Geol.* 69, 205–215. <https://doi.org/10.1016/j.marpetgeo.2015.10.022>.

- Xu, J., Wu, S., Liu, J., et al., 2021a. New insights into controlling factors of pore evolution in organic-rich shale. *Energy Fuel*. 35 (6), 4858–4873. <https://doi.org/10.1021/acs.energyfuels.0c04189>.
- Xu, L., Yang, K., Wei, H., et al., 2021b. Diagenetic evolution sequence and pore evolution model of mesoproterozoic xiamaling organic-rich shale in Zhangjiakou, Hebei, based on pyrolysis simulation experiments. *Mar. Petrol. Geol.* 132, 105233. <https://doi.org/10.1016/j.marpetgeo.2021.105233>.
- Yang, G., Wang, H., Shen, H., et al., 2015. Characteristics and exploration prospects of Middle Permian reservoirs in the Sichuan basin. *Nat. Gas. Ind. B.* 2 (5), 399–405. <https://doi.org/10.1016/j.ngib.2015.09.015>.
- Zhang, P., He, X., Gao, Q., et al., 2021. Geological characteristics and enrichment pattern of Permian Mao 1 member shale gas reservoirs at the Southeastern margin of Sichuan basin. *Oil Gas Geol.* 42 (1), 146–157. <https://doi.org/10.11743/ogg20210113>.
- Zhang, T., Ellis, G.S., Ruppel, S.C., et al., 2012. Effect of organic-matter type and thermal maturity on methane adsorption in shale-gas systems. *Org. Geochem.* 47, 120–131. <https://doi.org/10.1016/j.orggeochem.2012.03.012>.
- Zhao, Z., Littke, R., Zieger, L., et al., 2020. Depositional environment, thermal maturity and shale oil potential of the Cretaceous Qingshankou Formation in the eastern Changling Sag, Songliao Basin, China: an integrated organic and inorganic geochemistry approach. *Int. J. Coal Geol.* 232, 103621. <https://doi.org/10.1016/j.coal.2020.103621>.
- Zhou, J., Yao, G., Yang, G., et al., 2016. Lithofacies paleogeography and favorable gas exploration zones of Qixia and Maokou Fms in the Sichuan basin. *Nat. Gas. Ind. B.* 3, 226–233. <https://doi.org/10.1016/j.ngib.2016.05.007> (In Chinese).